ANTIOXIDANTS & REDOX SIGNALING
Volume 26, Number 17, 2017

DOI: 10.1089/ars.2016.6630

FORUM ORIGINAL RESEARCH COMMUNICATION

Nitric Oxide Regulates Skeletal Muscle Fatigue, Fiber Type, Microtubule Organization, and Mitochondrial ATP Synthesis Efficiency Through cGMP-Dependent Mechanisms

Younghye Moon,[1] Jordan E. Balke,[1] Derik Madorma,[1] Michael P. Siegel,[2] Gary Knowels,[2] Peter Brouckaert,[3] Emmanuel S. Buys,[4] David J. Marcinek,[2,5] and Justin M. Percival[1]

Abstract

Aim: Skeletal muscle nitric oxide–cyclic guanosine monophosphate (NO-cGMP) pathways are impaired in Duchenne and Becker muscular dystrophy partly because of reduced nNOSμ and soluble guanylate cyclase (GC) activity. However, GC function and the consequences of reduced GC activity in skeletal muscle are unknown. In this study, we explore the functions of GC and NO-cGMP signaling in skeletal muscle.
Results: GC1, but not GC2, expression was higher in oxidative than glycolytic muscles. GC1 was found in a complex with nNOSμ and targeted to nNOS compartments at the Golgi complex and neuromuscular junction. Baseline GC activity and GC agonist responsiveness was reduced in the absence of nNOS. Structural analyses revealed aberrant microtubule directionality in GC1$^{-/-}$ muscle. Functional analyses of GC1$^{-/-}$ muscles revealed reduced fatigue resistance and postexercise force recovery that were not due to shifts in type IIA–IIX fiber balance. Force deficits in GC1$^{-/-}$ muscles were also not driven by defects in resting mitochondrial adenosine triphosphate (ATP) synthesis. However, increasing muscle cGMP with sildenafil decreased ATP synthesis efficiency and capacity, without impacting mitochondrial content or ultrastructure.
Innovation: GC may represent a new target for alleviating muscle fatigue and that NO-cGMP signaling may play important roles in muscle structure, contractility, and bioenergetics.
Conclusions: These findings suggest that GC activity is nNOS dependent and that muscle-specific control of GC expression and differential GC targeting may facilitate NO-cGMP signaling diversity. They suggest that nNOS regulates muscle fiber type, microtubule organization, fatigability, and postexercise force recovery partly through GC1 and suggest that NO-cGMP pathways may modulate mitochondrial ATP synthesis efficiency. *Antioxid. Redox Signal*. 26, 966–985.

Keywords: nNOS, soluble guanylate cyclase, PDE5, mitochondria, microtubules, fatigue

Introduction

NEURONAL NITRIC OXIDE SYNTHASE (nNOS) splice variants, mu (nNOSμ) and beta (nNOSβ), synthesize the majority of NO in skeletal muscle. We reported that nNOSμ and nNOSβ-deficient (nNOS$\mu/\beta^{-/-}$) muscles exhibit impaired hypertrophic growth, severe weakness, exaggerated fatigue, poor force recovery after exercise, and qualitative defects in subsarcolemmal microtubule cytoskeleton organization (57). nNOS$\mu^{-/-}$ muscles show a substantial increase in type IIX fibers, while nNOS$\mu/\beta^{-/-}$ muscles show increased type IIB fibers content at the expense of type IIA fibers (54, 56, 57).

[1]Department of Molecular and Cellular Pharmacology, University of Miami Miller School of Medicine, Miami, Florida.
[2]Department of Bioengineering, University of Washington, Seattle, Washington.
[3]Department for Molecular Biomedical Research and Biomedical Molecular Biology, Ghent University, Ghent, Belgium.
[4]Department of Anesthesia, Critical Care and Pain Medicine, Anesthesia Center for Critical Care Research, Massachusetts General Hospital, Boston, Massachusetts.
[5]Department of Radiology, University of Washington, Seattle, Washington.

Innovation

Skeletal muscle nitric oxide–cyclic guanosine monophosphate (NO-cGMP) pathways are therapeutic targets in dystrophinopathies. However, the functions of key members of this pathway, soluble guanylate cyclase (GC) and phosphodiesterase 5 (PDE5), remain unknown. We show evidence that NO-cGMP signaling may differ between skeletal muscles and be facilitated by differential targeting of GC isoforms. We also provide evidence that GC1 may play important roles in muscle fatigue, plasticity, and microtubule organization. These findings suggest GC1 as a new target for alleviating muscle fatigue. We show that cGMP enhancement with sildenafil reduces mitochondrial adenosine triphosphate synthesis efficiency and capacity, suggesting a new role for PDE5 in mitochondrial bioenergetics.

The specific mechanisms by which nNOS enzymes regulate hypertrophy, fiber type, strength, fatigue resistance, and microtubule organization remain to be deciphered.

Four candidate mechanisms exist that may enable nNOS to regulate multiple physiological processes, sometimes simultaneously in skeletal muscle. The first mechanism is muscle-specific control of nNOS expression and activity where glycolytic muscles can have higher nNOSμ expression and activity than oxidative muscles (41). Note that glycolytic muscles exert fast contractions, fatigue rapidly, and are required for tasks involving strength and speed. Conversely, oxidative muscles exhibit slow contraction speeds, high resistance to fatigue, and are rich in mitochondria and capillaries. Oxidative muscles are important for maintaining posture and tasks involving endurance (8). The second mechanism is the dynamic activity-dependent control of nNOSμ localization (38, 71). The third mechanism is differential nNOS isozyme sorting to create spatially and functionally distinct nNOS splice variant compartments at the sarcolemma, Golgi complex, neuromuscular junction, and sarcoplasmic reticulum (2, 21, 41, 54, 57, 72). The fourth mechanism is the choice of target or effector for NO.

Soluble guanylate cyclase (GC) is a direct physiological target of NO (26). GC exists as two heterodimeric isoforms, GC1 and GC2, which comprise $\alpha1\beta1$ and $\alpha2\beta1$ GC subunits, respectively. Under resting conditions, GC synthesizes cyclic guanosine monophosphate (cGMP) at low rates; however, under activating conditions, additional NO binds GC substantially increasing cGMP synthesis (19). cGMP then activates proteins such as phosphodiesterase 5 (PDE5) and cGMP-activated protein kinase (PKG). Little is known about GC function in skeletal muscle, and it remains unknown which functions of nNOS are mediated by GC. However, expression of both GC1 and GC2 has been reported in skeletal muscle tissues, but reports conflict concerning GC1 localization at the sarcolemma (23, 28). In addition, current evidence suggests that GC1, nNOSμ, and PKG all localize to the neuromuscular junction (2, 16, 23).

Mitochondria represent another important target of NO-cGMP signaling. In skeletal muscle, NO is required for normal mitochondrial integrity and NO-cGMP signaling may regulate mitochondrial biogenesis, fission, and respiration in muscle cells (17, 18, 43, 52, 53, 57). Supraphysiological PKG overexpression drives the biogenesis of giant mitochondria *in vivo* (49). However, it remains unknown if NO-cGMP signaling controls biogenesis under more physiological conditions. In addition, it is not known if GC1 regulates skeletal muscle mitochondrial function or content.

NO-cGMP signaling can be terminated by PDE5 (25). PDE5 catabolizes a small fraction of total cGMP in skeletal muscle and its functions in skeletal muscle cells are poorly defined (9). However, PDE5 does not appear to regulate skeletal muscle strength and fatigue resistance (54, 60). In the dystrophin-deficient skeletal muscles of Duchenne and Becker muscular dystrophy (DBMD) patients and mdx mouse model of Duchenne muscular dystrophy (DMD), PDE5 plays clinically relevant roles in vasomodulation and fibrosis (6, 40, 47, 50, 55, 60). Inhibition of PDE5 with sildenafil partially restores defective NO-GC-cGMP signaling, thereby improving blood delivery and reducing fibrosis in dystrophic muscle (10, 13–15). Clinical testing is ongoing to evaluate PDE5 inhibition as a DBMD therapy. These findings underscore the translational importance of deciphering skeletal muscle GC and PDE5 function to clarify the role of impaired NO-cGMP signaling in DBMD disease pathogenesis.

In the present study, we explore NO-GC1-cGMP signaling in skeletal muscle using nNOS$^{-/-}$, GC1$^{-/-}$ mice, and the PDE5 inhibitor, sildenafil. We find that unlike nNOSμ, GC1 expression was highest in oxidative muscles and that GC1 was targeted to nNOS compartments at the Golgi complex and neuromuscular junction. Like nNOS$^{-/-}$ muscles, GC1$^{-/-}$ muscles fatigued more rapidly, exhibited poor force recovery after fatiguing exercise, and showed defects in microtubule assembly and shifts in type II fiber composition. These data suggested that nNOS regulates muscle contractility, fiber type, and microtubule assembly partly through GC1-dependent mechanisms. Reduced cGMP synthesis in GC1$^{-/-}$ muscles had no impact on mitochondria. However, increasing cGMP with sildenafil decreased the efficiency and capacity of mitochondrial adenosine triphosphate (ATP) synthesis, without impacting mitochondrial content or ultrastructure. These data provide the first evidence for PDE5 as a novel modulator of mitochondrial oxidative phosphorylation and a novel role for NO-cGMP signaling in skeletal muscle bioenergetics.

Results

nNOS activity and expression were reported to be higher in glycolytic than oxidative skeletal muscles; therefore, we hypothesized that GC expression may also differ between muscles (41). We found that the $\alpha1$GC and $\beta1$GC subunits of GC1 were expressed at a higher level in oxidative soleus and diaphragm muscles compared with more glycolytic gastrocnemius and tibialis anterior (TA) muscles (Fig. 1A, B). In contrast, expression of the $\alpha2$GC subunit of GC2 did not differ between muscles (Fig. 1C). These differences in GC enzyme expression between skeletal muscle types suggest greater cGMP synthesis capacity in oxidative muscles and potential muscle-specific differences in GC enzyme function and NO-cGMP signal propagation.

Another important characteristic of skeletal muscle NO signaling is that it is facilitated by nNOS isoform sorting. To test if GC enzyme sorting could also serve as a mechanism to enable nNOS signaling diversity (by restricting GC NO receptor localization), we investigated GC targeting to known nNOS compartments. The $\beta1$GC subunit colocalized with the

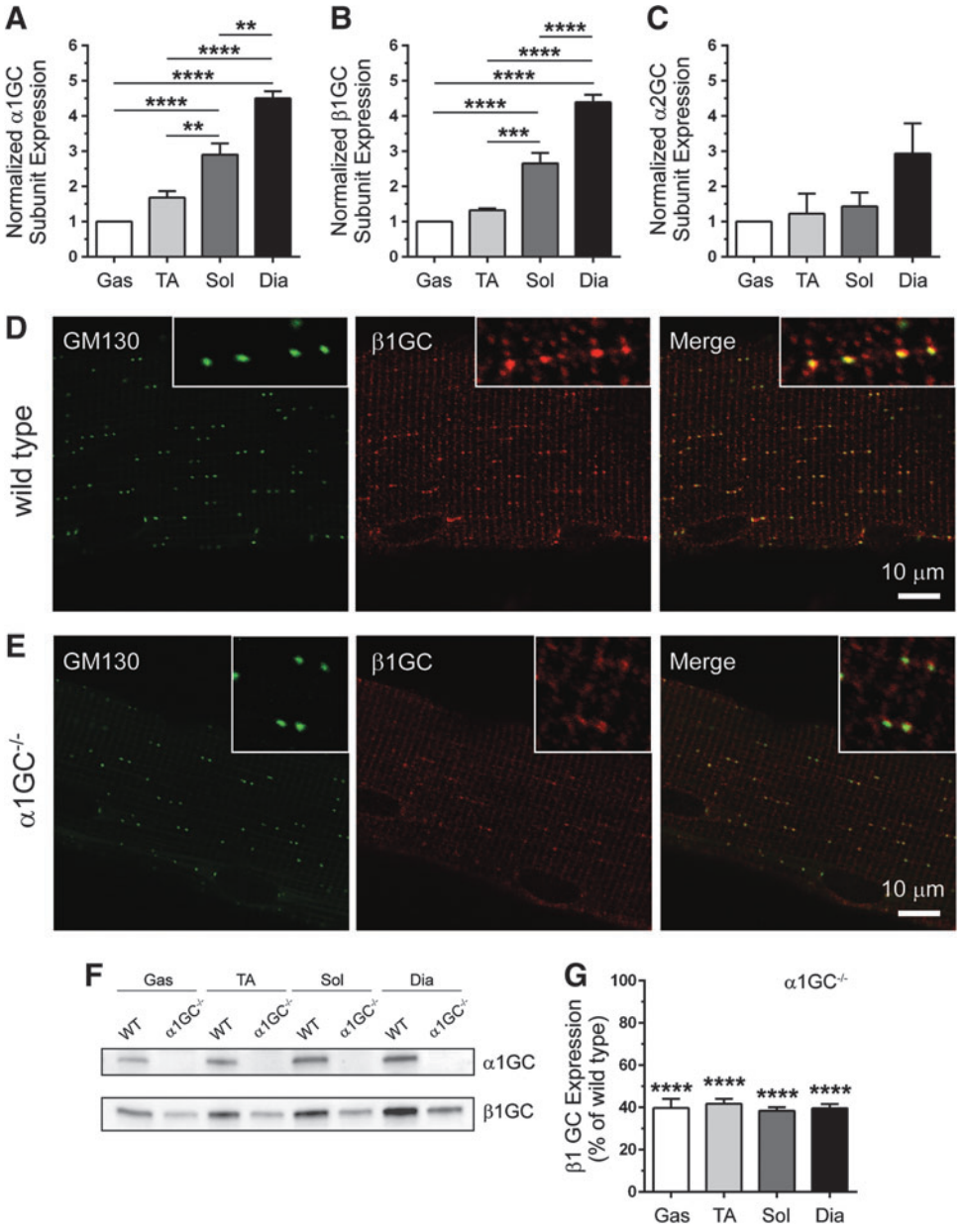

FIG. 1. GC expression differs between oxidative and glycolytic skeletal muscles and GC localizes to membranes of the *cis*-Golgi complex. **(A)** Quantitation of Western blots of α1GC subunit (GC1) expression in WT glycolytic (gastrocnemius and tibialis anterior) and oxidative (soleus and diaphragm) skeletal muscles from 3-month-old mice **(B)** Quantitation of Western blots of β1GC subunit expression in gas, TA, sol, and dia skeletal muscles from 3-month-old WT mice. **(C)** Quantitation of Western blots of α2GC subunit (GC2) expression in glycolytic and oxidative skeletal muscles from 2-month-old WT mice. In **(A–C)**, expression was normalized to mean gastrocnemius GC subunit expression. $n = 7$ for all groups. $^{**}p < 0.01$, $^{***}p < 0.001$, and $^{****}p < 0.0001$ by one-way ANOVA with Tukey's multiple comparison test. **(D)** Representative confocal micrographs showing colocalization (*right panel*) of the *cis*-Golgi complex marker, GM130 (*left panel*), and the β1GC subunit (*middle panel*) in a WT gastrocnemius myofiber. **(E)** Representative confocal micrographs of $\alpha1GC^{-/-}$ gastrocnemius myofiber showing normal GM130 labeling (*left panel*), but reduced *cis*-Golgi β1GC labeling (*middle panel*). For **(D, E)**, *insets* show a magnified view of Golgi labeling with $n \geq 6$ for WT and $\alpha1GC^{-/-}$ groups. **(F)** Representative Western blots of α1GC and β1GC expression in gas, TA, sol, and dia from WT and $\alpha1GC^{-/-}$ mice. **(G)** Quantitation of Western blots of β1GC expression in $\alpha1GC^{-/-}$ muscles. β1GC expression is expressed as mean percentage of WT. For **(F, G)**, $n = 7$ for both groups. $^{****}p < 0.0001$ by Student's unpaired *t*-test comparison of mean β1GC expression between WT and $\alpha1GC^{-/-}$ muscles. GC, soluble guanylate cyclase; Gas, gastrocnemius; TA, tibialis anterior; Sol, soleus; Dia, diaphragm; WT, wild-type. To see this illustration in color, the reader is referred to the web version of this article at www.liebertpub.com/ars

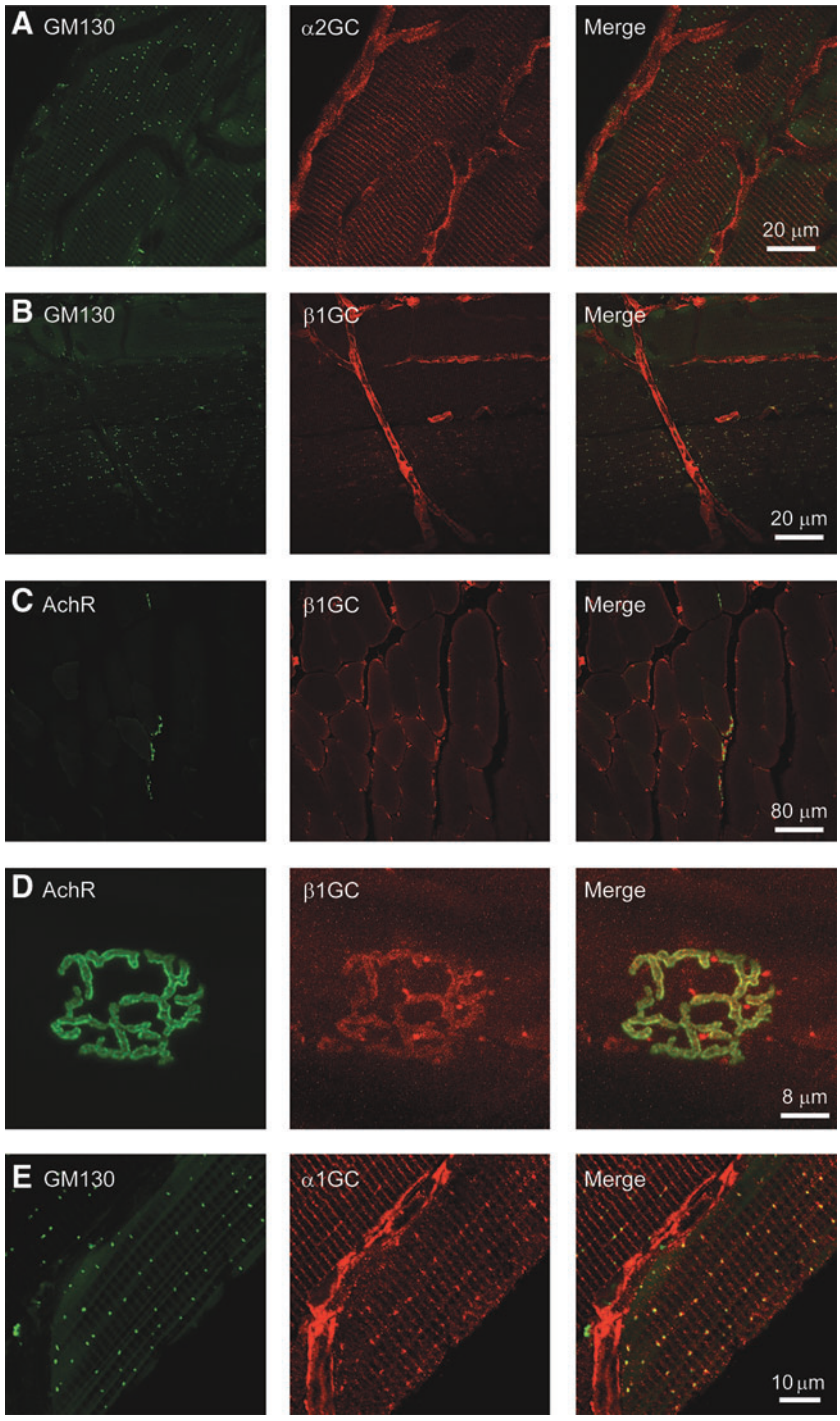

FIG. 2. GC is targeted to the neuromuscular synapse in muscle cells and expressed in muscle-associated microvasculature. (A) Representative confocal micrographs showing that α2GC subunit is not localized to the *cis*-Golgi complex marked by GM130, but is expressed in blood vessels closely associated with muscle cells in the tibialis anterior. Striated staining was also observed potentially representing another GC2 compartment. **(B)** Representative confocal micrographs showing that *β*1GC subunit localizes to the *cis*-Golgi complex marked by GM130 in myofibers and to muscle-associated blood vessels. **(C)** Representative confocal micrographs of a transverse section of gastrocnemius muscles coimmunolabeled with α-bungarotoxin to identify postsynaptic AchRs of the neuromuscular junction (*left panel*) and anti-*β*1GC antibodies (*middle panel*). *β*1GC was enriched at the neuromuscular junction (*right panel*) and in blood vessels, but did not localize to the sarcolemma. **(D)** Representative high-magnification confocal micrographs showing an *en face* view of the neuromuscular junction labeled with AchR (*left panel*) from a gastrocnemius myofiber. *β*1GC (*middle panel*) colocalized with AchR (*right panel*), indicating targeting of GC to the neuromuscular synapse. **(E)** Representative confocal micrographs showing that α1GC subunit is localized to the *cis*-Golgi complex marked by GM130 and to striations and blood vessels closely associated with individual muscle fibers in the tibialis anterior. For all groups, $n \geq 3$. AchR, acetylcholine receptor. To see this illustration in color, the reader is referred to the web version of this article at www.liebertpub.com/ars

cis-Golgi marker, GM130, in wild-type muscles where nNOS*β* was found (Fig. 1D) (57). *β*1GC subunit also localized to striations seen previously in cardiac muscle cells (12). Golgi-associated *β*1GC was reduced in GC1$^{-/-}$ muscles, likely due to reductions in *β*1GC expression; however, these data nonetheless support an association of GC1 with the *cis*-Golgi (Fig. 1E). Western blotting showed that loss of α1GC reduced *β*1GC expression by 60% (Fig. 1F, G). Similarly, the α1GC subunit also localized to the *cis*-Golgi and to other structures, including striations and neighboring blood vessels (Fig. 2E). Together, these data provide evidence that NO-sensitive GC1 may act as an effector for nNOS*β* at the *cis*-Golgi complex in skeletal muscle cells.

In contrast, the α2GC subunit of GC2 did not localize to the Golgi, but to striations (Fig. 2A). Blood vessels were also labeled with α1GC, α2GC, and *β*1GC subunit antibodies, indicating that GC1 and GC2 are expressed in the muscle vasculature (Fig. 2A, B, E). Importantly, *β*1GC was not expressed at the sarcolemma (Fig. 2C), but at blood vessels (puncta), and colocalized with acetylcholine receptors (AchR) on the postsynaptic muscle membranes at the neuromuscular junction (Fig. 2D). We were unable to

demonstrate α1GC or α2GC colocalization with AchR for reasons that are unclear (not shown). Thus, GC is situated close to nNOSμ at postsynaptic, but not sarcolemmal, membranes. AchR distribution was unaffected by the loss of nNOS (Supplementary Fig. S1G; Supplementary Data are available online at www.liebertpub.com/ars). Together, these data indicate that GC is targeted to a subset of nNOS compartments, supporting the control of GC sorting as a mechanism to generate nNOS signaling diversity and suggesting a dependence of GC function on nNOS.

To test the dependence of cGMP synthesis by GC on nNOS, we investigated GC activity at baseline and in response to agonists in $nNOS^{-/-}$ muscles. Basal GC activity was reduced to a similar extent in $nNOS^{-/-}$ and $GC1^{-/-}$ TA muscles relative to wild-type controls (Fig. 3A). However, baseline GC activity was significantly reduced in $GC1^{-/-}$, but not $nNOS^{-/-}$, soleus muscles (Fig. 3C). Differences in basal GC activity between $nNOS^{-/-}$ TA and soleus muscles may be due to greater vascularization of the soleus with higher nonmuscle resting GC activity. These data indicate that GC1 is a significant cGMP source in both resting TA and soleus muscles and that baseline GC1 activity is nNOS dependent in TA muscles.

We then tested the nNOS dependence of GC activation by distinct agonists, including the NO donor, DETANO, the GC activator, BAY 58-2667 (BAY 58), and the GC stimulator, BAY 41-2272 (BAY 41) (22, 24, 70). GC activation by DETANO, BAY 58, or BAY 41 was decreased in $nNOS^{-/-}$ TA muscles (Fig. 3A). Indeed, GC activity was not significantly different between agonist-treated $nNOS^{-/-}$ and $GC1^{-/-}$ TA muscles. Remarkably, these data suggest that nNOS-dependent activation of GC cannot be fully mimicked by addition of exogenous NO and that BAY 41 may not be fully NO independent in glycolytic skeletal muscle. Similar trends in GC agonist responsiveness were seen in the soleus, except that BAY 41 stimulated GC to wild-type levels (Fig. 3C). Normalization of DETANO, BAY 58, and BAY 41 agonist-induced GC activity to baseline activity in the TA and soleus showed similar trends reflecting the strong nNOS dependence of GC activation (Fig. 3B, D).

We then tested decreased GC subunit expression as a mechanism for reducing GC activity and agonist responsiveness. Western blotting revealed that α1, β1, and α2GC subunit expression was not decreased in $nNOS^{-/-}$ gastrocnemius, TA, soleus, or diaphragm muscles (Fig. 3E–G and Supplementary Fig. S1A). On the contrary, α1 and β1GC exhibited a compensatory increase in both gastrocnemius and diaphragm muscles (Fig. 3E, F). Therefore, reduced GC activity in $nNOS^{-/-}$ muscles was not caused by decreased GC subunit expression. Importantly, these data collectively suggest that GC activity is strongly nNOS dependent and that GC1 inhibition may contribute to skeletal muscle dysfunction in $nNOS^{-/-}$ mice.

To further understand the regulation of sGC activity by nNOS, we investigated whether sGC and nNOS could exist in a cytosolic complex by immunoprecipitation analysis. The anti-α1GC antibody could immunoprecipitate nNOSμ in WT, but not $nNOS^{-/-}$, diaphragm muscles (Fig. 3H). Similar results were observed in TA muscles (not shown). The converse immunoprecipitation was unsuccessful. These findings suggest that α1β1 sGC and nNOSμ exist in a complex together in the cytoplasm, which may facilitate the regulation of sGC by nNOS.

Given that loss of nNOS impaired baseline GC activity and agonist responsiveness, we investigated if the converse was possible that loss of GC may reduce nNOS activity. Because it is not possible to specifically measure nNOS activity alone *in vivo*, we evaluated the fraction of active serine1446 phosphorylated nNOSμ, the primary enzymatic NO source in muscle (34, 61). Loss of GC1 decreased the fraction of active serine1446 phosphorylated nNOSμ by 40% (Supplementary Fig. S1B). These findings suggest a negative feedback loop between nNOSμ and GC1, whereby loss of GC1 activity attenuates upstream nNOSμ activity.

The dependence of GC activity on nNOS suggested that inhibition of GC1 could contribute to muscle dysfunction in $nNOS^{-/-}$ mice; therefore, we investigated possible functions of nNOS that could be mediated by GC1. Male and female $nNOS^{-/-}$ mice were previously shown to exhibit stunted growth (57). However, growth of male and female $GC1^{-/-}$ mice was similar to wild type, suggesting that growth defects in $nNOS^{-/-}$ mice were not due to impaired GC1 activity (Fig. 4A) (30, 57). Dual-energy X-ray absorptiometry indicated decreased body fat in male $GC1^{-/-}$ mice (Fig. 4B), while bone mineral density was unaffected (Fig. 4C). $nNOS^{-/-}$ TA masses were reported to be very low due to reduced muscle cell size marked by reduced feret diameter and cross-sectional area (57). However, $GC^{-/-}$ mice exhibited normal absolute TA masses and body weight normalized TA masses (Fig. 4D, E, respectively). These findings suggest that a global increase in male skeletal muscle mass was not solely responsible for the reduction in body fat percentage. Consistent with normal muscle growth, $GC1^{-/-}$ muscle cells were of normal size and exhibited no evidence of myopathy, dystrophy, or atrophy (Fig. 4F and Supplementary Fig. S1C, D). Accordingly, central nucleation, a biomarker of muscle cell degeneration/regeneration, was also normal in $GC1^{-/-}$ muscle (Fig. 4G). Feret diameters and cross-sectional areas of TA muscle cells in $GC^{-/-}$ mice were similar to controls, providing further evidence of normal $GC^{-/-}$ muscle growth (Fig. 4H, I, respectively). Importantly, these data suggest that GC1 is dispensable for normal skeletal muscle growth and that impaired hypertrophic growth in $nNOS^{-/-}$ mice was not due to inhibition of GC1 activity (57).

In addition to impairing muscle growth, $nNOS^{-/-}$ deficiency was shown to qualitatively disrupt the subsarcolemmal microtubule lattice (Fig. 5A, B) (57). To quantitate the impact of nNOS deficiency on microtubules, subsarcolemmal microtubule lattice directionality was analyzed using custom-built texture detection (TedT) software (Fig. 5C–E) (44). Loss of nNOS quantitatively disrupted subsarcolemmal microtubule organization (Fig. 5C). General microtubule directionality (D) was reduced by 50% in $nNOS^{-/-}$ TA muscle, reflecting impaired microtubule alignment (Fig. 5D). nNOS deficiency reduced the number of transverse microtubules oriented at 90° to the myofiber long axis (Fig. 5C). Accordingly, vertical directionality (D_v) was reduced by 84%, suggesting extreme disarray of transverse microtubules (Fig. 5E). Loss of directionality was partly attributable to a 41% reduction in subsarcolemmal microtubule density in $nNOS^{-/-}$ muscle (Fig. 5F).

To test if impaired subsarcolemmal microtubule organization in $nNOS^{-/-}$ muscles could be due to GC1 inhibition, we determined microtubule directionality and density in $GC1^{-/-}$ TA muscles. Confocal microscopic analyses showed that the subsarcolemmal microtubule lattice was qualitatively

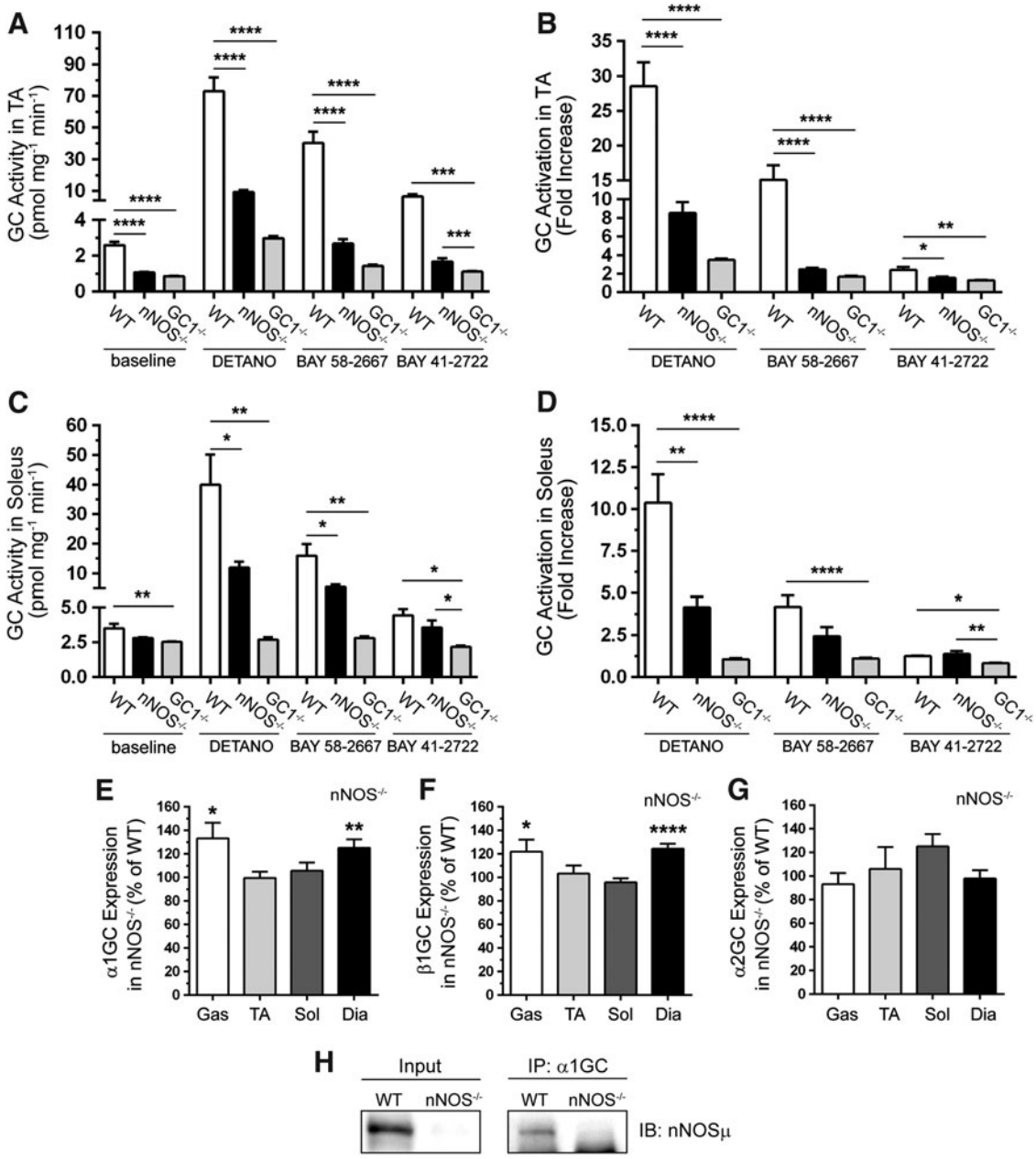

FIG. 3. Resting GC activity and responsiveness to DETANO, BAY 58-2667, and BAY 41-2722 agonists are nNOS dependent. **(A)** cGMP synthesis by GC at baseline and in response to NO donor, DETANO, the GC activator, BAY 58-2667, and GC stimulator, BAY 41-2722, agonists in 2-month-old glycolytic TA muscles from WT, nNOS$^{-/-}$, and α1GC$^{-/-}$ mice now referred to as GC1$^{-/-}$ mice. **(B)** Fold increase in TA muscle GC activity compared with baseline. **(C)** GC activity at baseline and in response to DETANO, BAY 58-2667, and BAY 41-2722 in 2-month-old oxidative soleus muscles from WT, nNOS$^{-/-}$, and GC1$^{-/-}$ mice. **(D)** Fold increase in soleus GC activity compared with baseline. **(E)** Quantitation of Western blots evaluating α1GC expression in nNOS$^{-/-}$ glycolytic (gastrocnemius and TA) and oxidative (soleus and diaphragm muscles). α1GC subunit expression in nNOS$^{-/-}$ muscles is expressed as percent of WT. **(F)** Western blot-based quantitation of β1GC subunit expression in nNOS$^{-/-}$ muscles. β1GC expression is expressed as percent of WT. **(G)** Quantitation of Western blots of α2GC subunit expression in nNOS$^{-/-}$ muscles. α2GC expression is expressed as percent of WT. For **(A–G)**, $n = 8$ for all groups. For **(A–D)**, $^{*}p < 0.05$, $^{**}p < 0.01$, $^{***}p < 0.001$, and $^{****}p < 0.0001$ by one-way ANOVA with Tukey's multiple comparison test. For **(E–G)**, $^{*}p < 0.05$, $^{**}p < 0.01$, and $^{****}p < 0.0001$ by Student's unpaired *t*-test comparison of mean β1GC expression between WT and nNOS$^{-/-}$ muscles. **(H)** Representative blots of immunoprecipitation analyses showing that α1GC can immunoprecipitate nNOSμ from WT, but not nNOS$^{-/-}$ diaphragm muscle. $n = 4$.

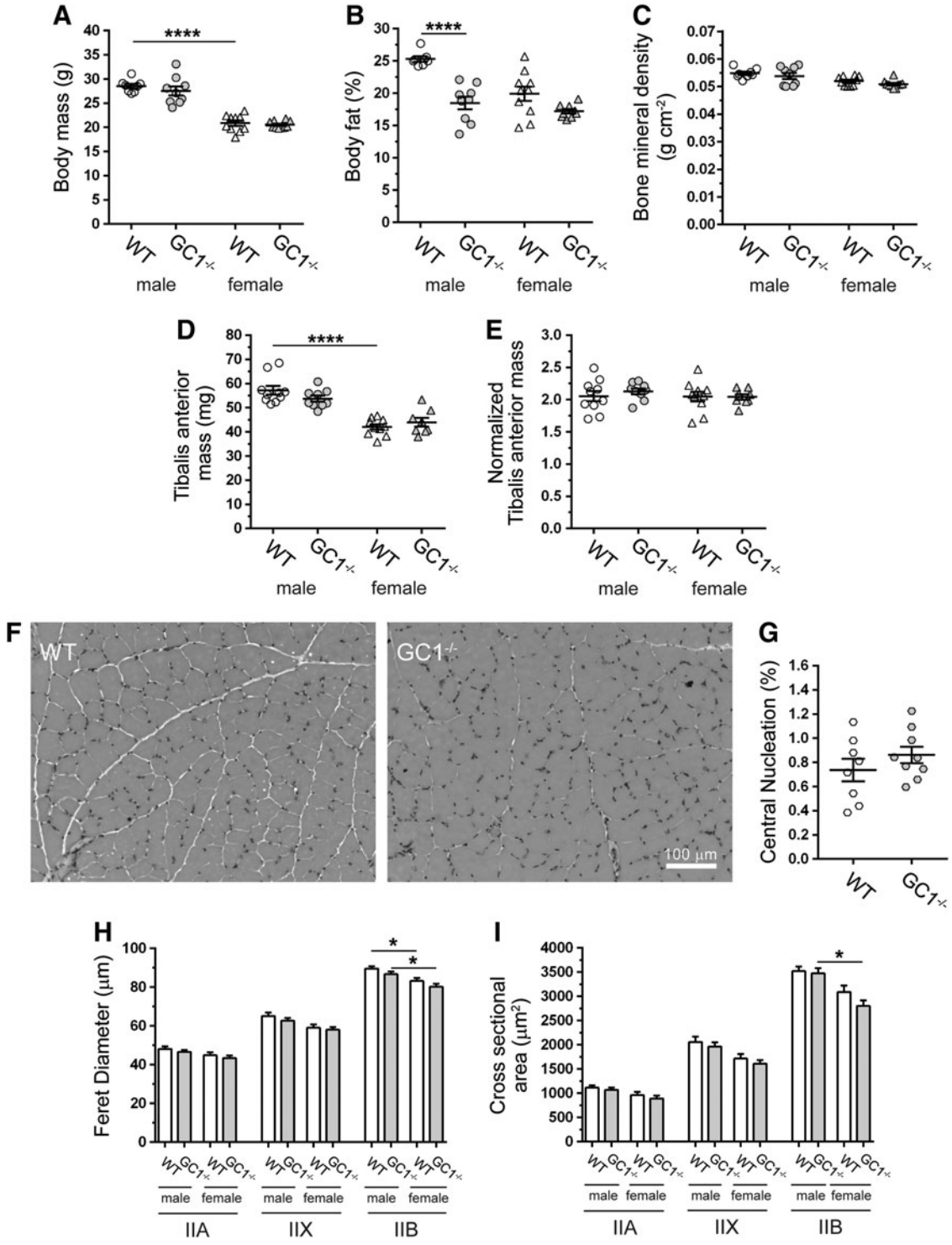

FIG. 4. GC1$^{-/-}$ mice exhibit sex-specific reductions in body fat and normal skeletal muscle cell hypertrophy. **(A)** Body weights of male and female WT and GC1$^{-/-}$ mice. **(B)** Body fat percentage in male and female WT and GC1$^{-/-}$ mice measured by DEXA. **(C)** DEXA measurement of bone mineral density in male and female WT and GC1$^{-/-}$ mice. **(D)** TA muscle mass in WT and GC1$^{-/-}$ mice. **(E)** TA muscle mass normalized to body mass. **(A–E),** $n = 8$–10 for all groups. **(F)** Representative bright-field micrographs of hematoxylin and eosin-stained TA muscles from male WT and GC1$^{-/-}$ mice. $n \geq 6$. **(G)** The percentage of centrally nucleated muscle fibers in WT and GC1$^{-/-}$ TA muscles. $n = 8$ for WT and 9 for GC$^{-/-}$ groups. **(H)** Feret diameters of type IIA, IIX, and IIB-positive TA muscle cells in male and female WT and GC1$^{-/-}$ mice. **(I)** Cross-sectional areas of type IIA, IIX, and IIB fibers in TA muscles from male and female WT and GC1$^{-/-}$ mice. **(H, I)**, $n = 5$ for all groups. For **(A–E)**, **(H, I)**, $^{*}p < 0.05$, and $^{****}p < 0.0001$ from regular two-way ANOVA using sex and genotype as variables and Tukey's *post hoc* test. DEXA, dual-energy X-ray absorptiometry.

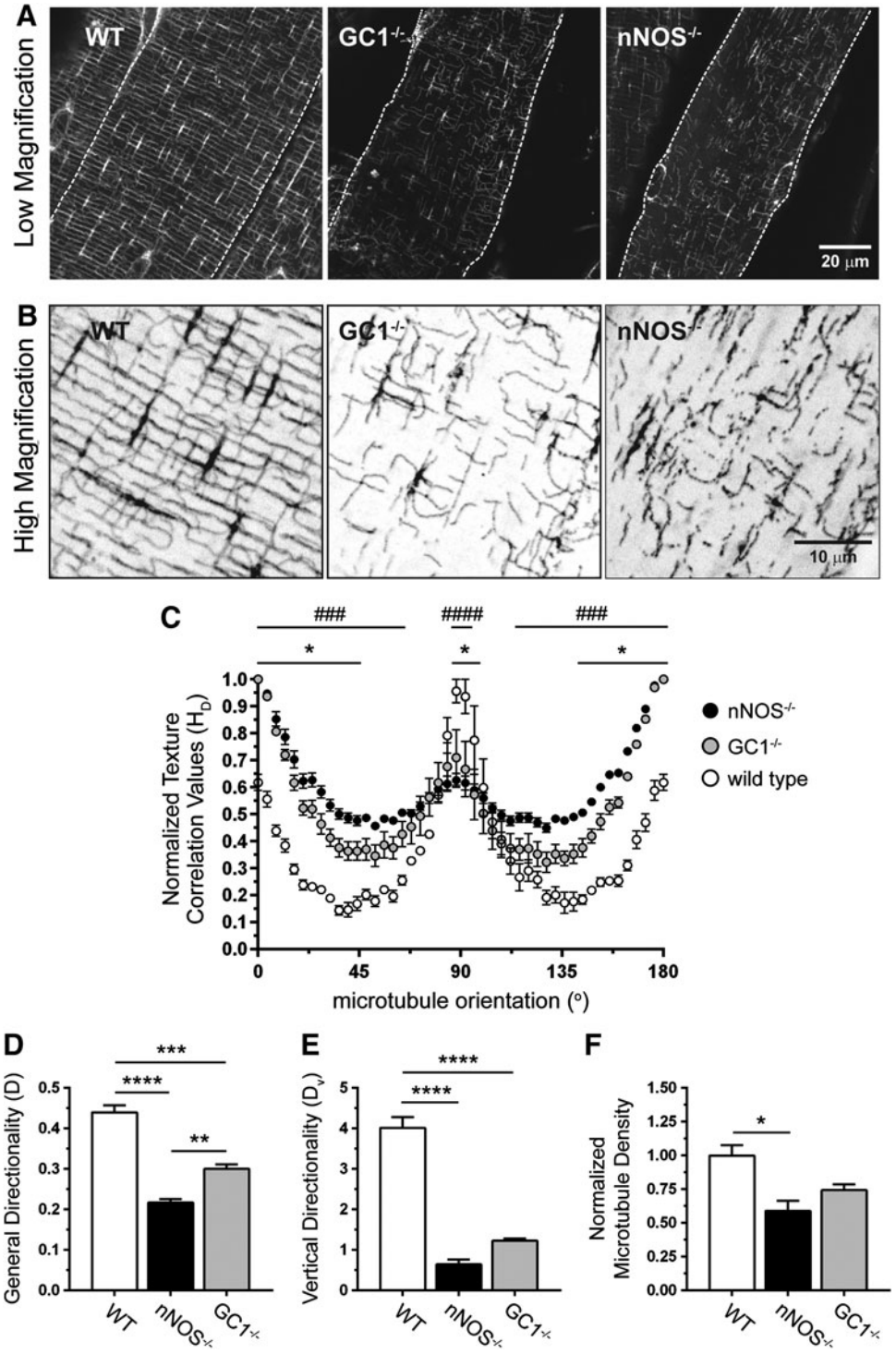

FIG. 5. nNOS regulates subsarcolemmal microtubule lattice organization through a GC1-cGMP-dependent mechanism. (A) Representative low-magnification confocal micrographs of the subsarcolemmal microtubule cytoskeleton immunolabeled with FITC-conjugated anti-α-tubulin antibody in TA myofibers from WT, $GC1^{-/-}$, and $nNOS^{-/-}$ mice. **(B)** High-magnification versions of regions within the confocal micrographs in **(A)**. **(C)** Histogram of subsarcolemmal microtubule general directionality in TA myofibers from WT, $GC1^{-/-}$, and $nNOS^{-/-}$ mice. **(D)** Subsarcolemmal general microtubule directionality scores in WT, $GC1^{-/-}$, and $nNOS^{-/-}$ TA muscles. **(E)** Quantitation of vertical (microtubules orthogonal to the myofiber long axis) microtubule directionality (D_v) in WT, $GC1^{-/-}$, and $nNOS^{-/-}$ TA myofibers. **(F)** Quantitation of subsarcolemmal microtubule densities in TA myofibers from WT, $GC1^{-/-}$, and $nNOS^{-/-}$ mice. **(A–F)**, $n = 3$–4 for all groups. For **(C)**, $^{###}p < 0.001$; $^{####}p < 0.0001$ for WT *versus* $nNOS^{-/-}$; and $^{*}p < 0.05$ for WT *versus* $GC^{-/-}$ from regular two-way ANOVA using orientation and genotype as variables with Tukey's multiple comparison test. For **(D–F)**, $^{*}p < 0.05$, $^{**}p < 0.01$, $^{***}p < 0.001$, and $^{****}p < 0.0001$ by one-way ANOVA with Tukey's multiple comparison test.

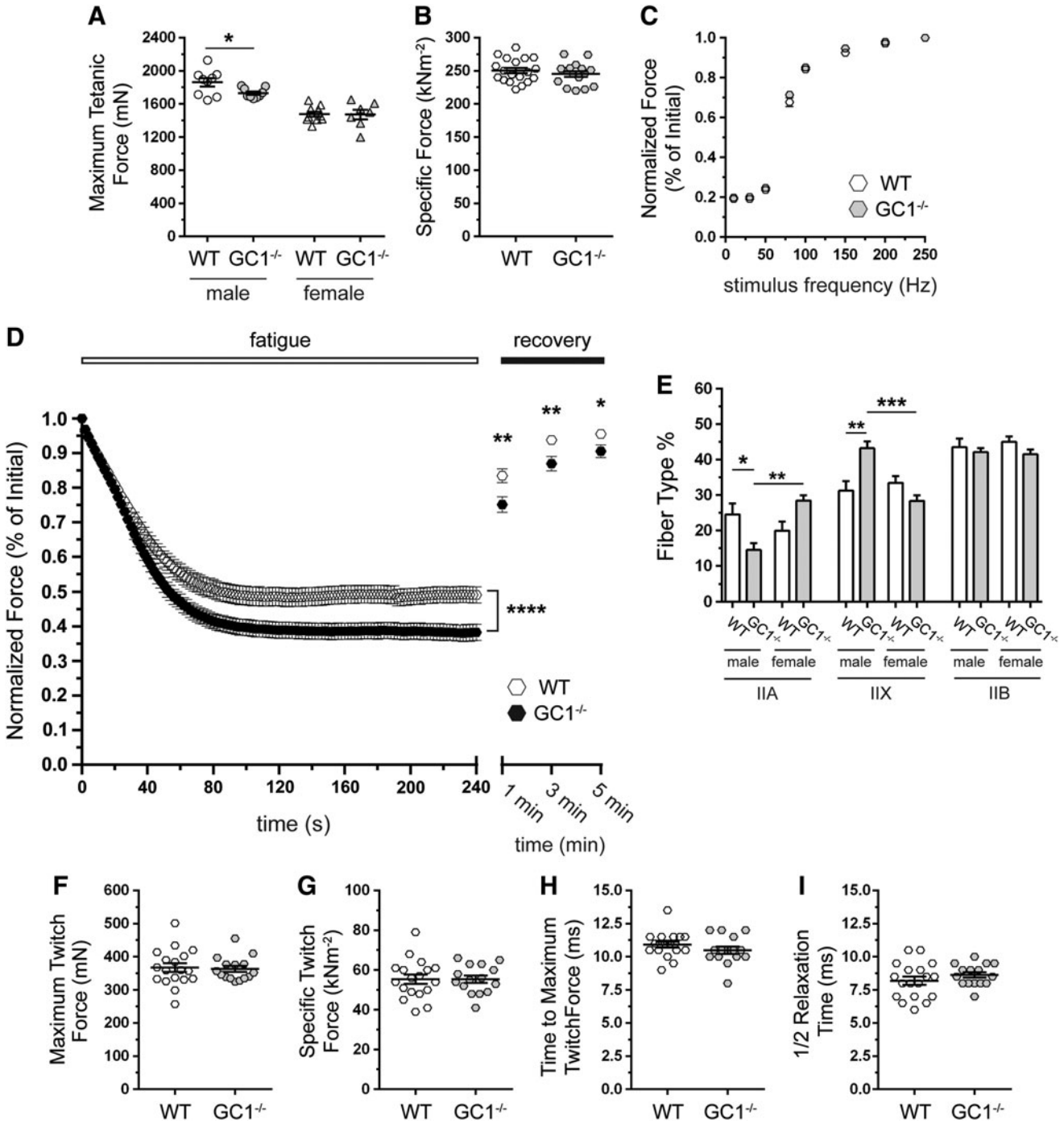

FIG. 6. GC1 is indispensable for normal skeletal muscle fatigue resistance. The isometric tetanic contractile properties of TA muscles in male and female WT and GC1$^{-/-}$ mice *in situ*. $n = 9$ for male groups, $n = 10$ and 7 for female WT and GC1$^{-/-}$ groups, respectively. **(A)** Maximal tetanic isometric force output. **(B)** Specific force output. $n = 19$ for WT and 16 for GC1$^{-/-}$ groups. **(C)** Normalized force–stimulation frequency relationship in WT and GC1$^{-/-}$ TA muscles. $n = 18$ per group. **(D)** Contraction-induced fatigue resistance. $n = 39$ and 34 for WT and GC1$^{-/-}$ groups, respectively. **(E)** Fiber composition in TA muscles from male and female WT and GC1$^{-/-}$ mice. $n = 7$ and 6 for male and female groups, respectively. Isometric twitch contractile properties of TA muscles from WT and GC1$^{-/-}$ male and female mice. **(F)** Maximum isometric twitch force output, **(G)** specific isometric twitch force output, **(H)** time to maximum isometric twitch force, and **(I)** time taken for muscle force to return to half maximum twitch force (½ relaxation time) in WT and GC1$^{-/-}$ TA muscles. For **(F–I)**, $n = 9$ male WT groups. $n = 10$ and 7 for female WT and GC1$^{-/-}$ groups, respectively. **(A, D, E)** $^{*}p < 0.05$; $^{**}p < 0.01$; and $^{***}p < 0.001$ from regular two-way ANOVA using sex and genotype **(A, E)** or genotype and time **(D)** or as variables with Tukey's multiple comparison test.

disrupted in $GC1^{-/-}$ muscles (Fig. 5A, B). This was confirmed by quantitative image analysis, which showed that GC1 deficiency disrupted microtubule organization (general directionality) to a degree intermediate between wild-type and $nNOS^{-/-}$ muscles (Fig. 5C, D). This suggests why microtubule-scaffolded Golgi complex localization was relatively normal in $GC^{-/-}$, but not in $nNOS^{-/-}$, muscles, as previously reported (Fig. 1E) (57). In addition, microtubules aligned at 90° to the long axis of the muscle fiber were similarly disrupted in $GC^{-/-}$ and $nNOS^{-/-}$ muscles indicated by decreased vertical directionality scores (Fig. 5E). Unlike loss of nNOS, GC1 deficiency did not significantly reduce microtubule density, suggesting a primary role for GC1 in microtubule orientation (Fig. 5F). Together with the nNOS-dependent of sGC activity, these data suggest that GC1-dependent nNOS signaling may play a role in regulating subsarcolemmal microtubule cytoskeleton organization in skeletal muscle cells.

We next explored the consequences of GC1 deficiency on muscle contractile performance by stimulating the TA muscle to contract *in situ* in anesthetized mice through electrical activation of the peroneal nerve. $nNOS^{-/-}$ TA muscles exhibit severe reductions in maximal tetanic force, specific force, and fatigue resistance (57). Therefore, given diminished GC1 activity in $nNOS^{-/-}$ muscles, we tested if GC1 inhibition could recapitulate the pronounced weakness of $nNOS^{-/-}$ mice. Maximum tetanic force output was modestly reduced in male, but not female, $GC1^{-/-}$ muscle (Fig. 6A). However, specific force output from male and female $GC1^{-/-}$ muscles was normal (Fig. 6B and Supplementary Fig. S2A). These findings argue that GC1 is dispensable for muscle strength and that muscle weakness in $nNOS^{-/-}$ mice was not due to GC1 inhibition.

The neuromuscular junction localization of GC suggested a role in motor neuron–muscle communication (Fig. 2D); therefore, we investigated force output at different peroneal nerve stimulation frequencies (Fig. 6C). Normalized force–frequency relationships were indistinguishable between control and $GC1^{-/-}$ muscles consistent with normal neuromuscular transmission (Fig. 6C and Supplementary Fig. S2B, C). However, male and female $GC1^{-/-}$ TA muscles could not sustain normal force output during repeated stimulation, indicating poor fatigue resistance (Fig. 6D and Supplementary Fig. S2D, E). Importantly, force output was depressed for 5 min after the fatigue period, indicating impaired postexercise force recovery (Fig. 6D). Importantly, $GC1^{-/-}$ muscle fatigue was not as severe as previously reported in $nNOS^{-/-}$ mice, suggesting partial compensation by GC2 and/or that nNOS regulates fatigue partly through a GC1-independent mechanism (57). Nonetheless, these data suggest that NO-GC1-cGMP signaling plays an important role in muscle fatigue resistance and postexercise force recovery.

Skeletal muscle fatigue resistance depends partly on fiber-type composition, with less fatigue-resistant muscles containing a greater ratio of glycolytic to oxidative fiber types (63). In addition, nNOS enzymes regulate type II fiber composition (57). Therefore, we investigated whether GC1 could also play a role in type II fiber-type specification and whether changes in fiber type could contribute to reduced $GC1^{-/-}$ muscle fatigue resistance. Loss of GC1 significantly decreased type IIA content by 41% in males, but increased it by 42% in female TA muscles, although this increase did not reach statistical significance (Fig. 6E). Male $GC1^{-/-}$ mice showed a 42% increase in type IIX fibers; however, type IIX content in $GC1^{-/-}$ females was unaffected (Fig. 6E). Type IIB fiber composition was unaffected in $GC1^{-/-}$ muscles. Together, these data indicate sex-specific regulation of oxidative type II fiber composition by GC1. However, these changes in fiber content are modest and unlikely to impact muscle fatigue resistance or contractility. To gain additional evidence that altered fiber composition did not impact contractility, we determined the twitch properties of $GC1^{-/-}$ TA muscles. Maximum twitch force, specific twitch force, time to maximum twitch force, and time to reach ½ maximum twitch force (½ relaxation time) were all unaffected in $GC1^{-/-}$ muscles (Fig. 6F–I, respectively). Collectively these data argue that altered type II fiber composition is not driving the lowered muscle fatigue resistance of $GC1^{-/-}$ mice.

We next explored deficits in mitochondrial ATP synthesis as a potential mechanism for the reduced muscle fatigue resistance of $GC1^{-/-}$ mice. Because mitochondria are regulated by NO and play a central role in skeletal muscle contractile performance, we tested if mitochondrial oxidative phosphorylation was impacted by GC1 inhibition using *in vivo* metabolic spectroscopy (5, 17, 18, 52, 53, 57, 67). Mitochondrial ATP synthesis (Fig. 7A), which is directly proportional to ATPase activity, and mitochondrial O_2 consumption (Fig. 7B) were unaffected in resting $GC1^{-/-}$ skeletal muscles. Accordingly, the P/O coupling ratio, an index of how tightly ATP generation is coupled to O_2 consumption, was similar between controls and $GC1^{-/-}$ mice (Fig. 7C). Maximal mitochondrial ATP synthesis capacity (ATP_{max}, Fig. 7D) and phosphocreatine-to-ATP metabolite ratios (PCr/ATP) were also unaffected in $GC1^{-/-}$ muscles (Fig. 7E). Taken together, these data suggested that GC1 is dispensable for mitochondrial ATP synthesis in resting skeletal muscle.

We next investigated if preservation of mitochondrial ATP synthesis in $GC1^{-/-}$ muscles was due to compensatory increases in mitochondrial content. Western blotting showed that expression of mitochondrial marker, VDAC1 (Fig. 7F), and specific subunits of respiratory complexes I through V (Fig. 7G) was unaffected in $GC1^{-/-}$ TA muscles (Fig. 7). Similar results were observed in gastrocnemius and soleus muscles (Supplementary Fig. S3A–D). Accordingly, expression of mitochondrial biogenesis regulator PGC1α mRNA was similar between wild-type and $GC1^{-/-}$ muscles (Fig. 7H). Together, these findings suggest that preservation of mitochondrial ATP synthesis in $GC1^{-/-}$ mice was not due to biogenesis. This loss-of-function approach also suggested that cGMP synthesis by GC1 is dispensable for establishing muscle mitochondrial content.

In skeletal muscle, cGMP synthesized by GC is broken down by several phosphodiesterases, including cGMP-activated and cGMP-specific PDE5 (9, 55, 60). To further understand the regulation of muscle mitochondrial function by cGMP, we used a gain-of-function approach to raise skeletal muscle cGMP by treating wild-type mice with the PDE5 inhibitor, sildenafil. Sildenafil treatment increased skeletal muscle cGMP twofold (Fig. 8L) (60). Sildenafil reduced the P/O coupling ratio by 40%, indicating partial uncoupling of O_2 consumption from ATP generation (Fig. 8A). The reduced P/O indicated very inefficient ATP synthesis where mitochondria were oxidizing more fuel substrates to

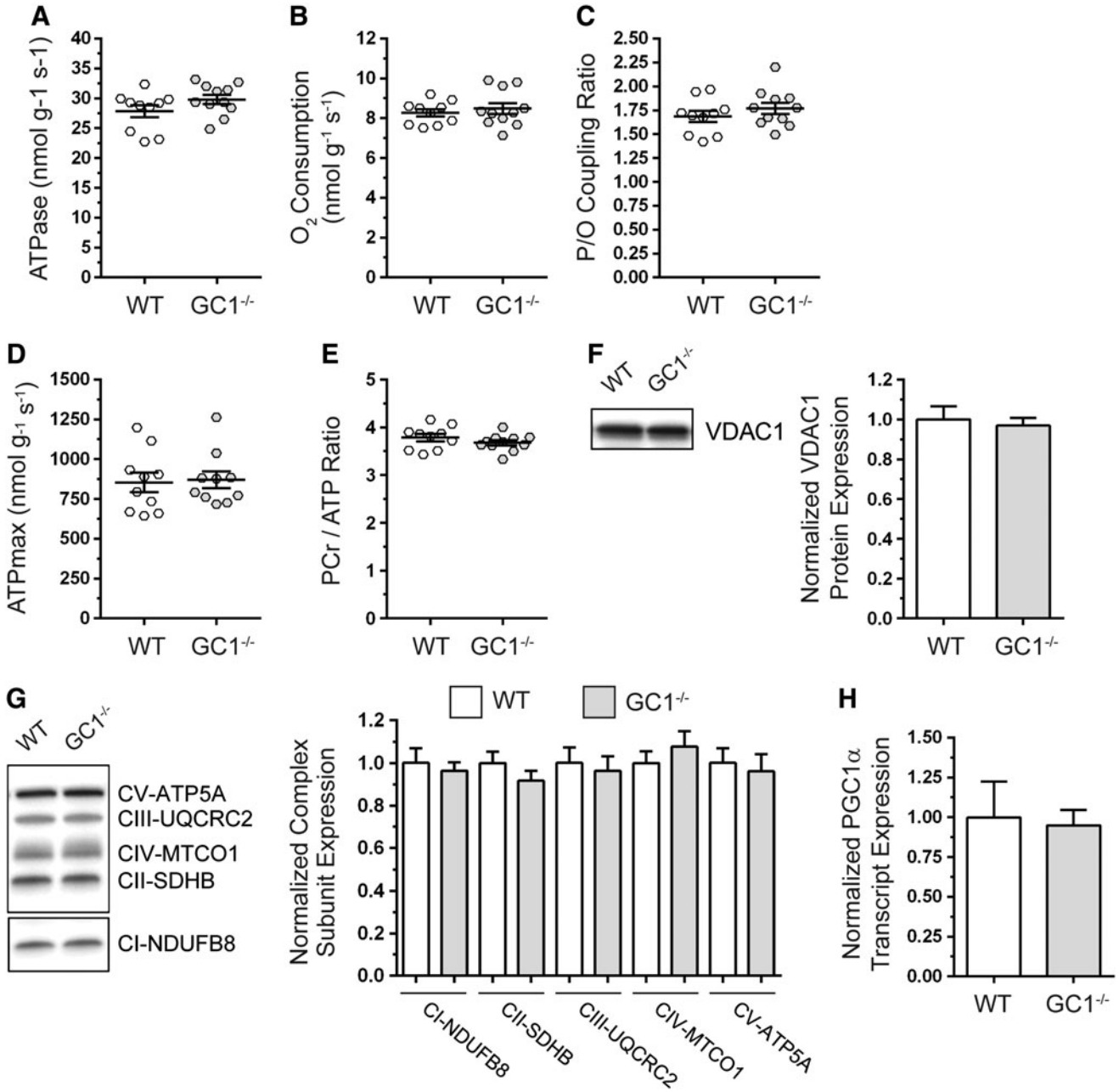

FIG. 7. GC1 is dispensable for resting skeletal muscle mitochondrial ATP synthesis and content. Mitochondrial ATP generation and oxygen consumption in hind limb skeletal muscles of anesthetized WT and GC1$^{-/-}$ mice were simultaneously measured by *in vivo* ^{31}P magnetic resonance and optical spectroscopy. **(A)** Mitochondrial ATP synthesis, which is directly proportional to ATPase activity. **(B)** Mitochondrial oxygen consumption rate. **(C)** Mitochondrial ATP synthesis efficiency as determined from the P/O coupling ratio, where P (ATP generation) is divided by oxygen consumption rate (O). **(D)** Mitochondrial ATP synthesis capacity (ATPmax). **(E)** Phosphocreatine-to-ATP ratio. For **(A–E)**, $n = 9$–10 for WT and 10–11 for GC1$^{-/-}$ groups, respectively. **(F)** Representative Western blot and densitometric quantitation of mitochondrial marker VDAC1 expression in tibialis anterior muscles. $n = 5$ for WT and GC1$^{-/-}$ groups. **(G)** Representative Western blot and densitometric quantitation of mitochondrial respiratory complex subunit expression in tibialis anterior muscles. **(H)** Quantitation of PGC1α transcript expression by qPCR. For **(G, H)**, $n = 6$ for WT and GC1$^{-/-}$ groups.

generate the same amount of ATP. Reduced P/O was caused by a decrease in ATP generation (Fig. 8B) and a concomitant increase in O_2 consumption (Fig. 8C). Inefficient ATP synthesis predictably reduced maximal mitochondrial ATP synthesis capacity (Fig. 8D). The reprogramming of mitochondrial oxidative phosphorylation was accompanied by a decrease in the PCr/ATP ratio, driven by a reduction in phosphocreatine (PCr) without impacting ATP levels (Fig. 8E–G). PCr is an important buffer of ATP levels; therefore, decreased PCr likely reflects an adaptive response to preserve skeletal muscle ATP.

Given that increases in cGMP may drive mitochondrial biogenesis in muscle cells, we tested if sildenafil-driven reductions in ATP synthesis efficiency and capacity were

accompanied by increased mitochondrial content using Western blotting and quantitative electron microscopy-based stereology (59). Expression of VDAC1 protein (Fig. 8H) and specific subunits of respiratory complexes I through V (Fig. 8I) were unaffected by sildenafil. In agreement, intermyofibrillar mitochondrial volume density (Fig. 8J) and subsarcolemmal mitochondrial pool densities (Fig. 8K) were similar between untreated and sildenafil-treated mice. In addition to regulating biogenesis, NO-cGMP signaling may also modulate mitochondrial size (17, 49). Therefore, we evaluated the impact of increased cGMP on intermyofibrillar and subsarcolemmal mitochondria ultrastructure by transmission electron microscopy (Supplementary Fig. S4). Sildenafil had no impact on the gross morphology of intermyofibrillar or subsarcolemmal mitochondria. Together, these data demonstrate that increasing cGMP with sildenafil does not impact muscle mitochondrial morphology or content. Importantly, these findings provide new evidence that NO-cGMP pathways regulated by PDE5 modulate skeletal muscle mitochondrial ATP synthesis efficiency and capacity.

Discussion

While skeletal muscle nNOS-GC-cGMP signaling is severely disrupted in DBMD, the functional consequences of this disruption remain to be deciphered. We provide new insights into the physiological functions of nNOS-GC-cGMP signaling in skeletal muscle that may advance understanding of how defects in this pathway promote disease pathogenesis in DBMD. These insights are based on findings suggesting that nNOS regulates muscle fatigue resistance, fiber specification, and microtubule organization partly through GC1. Our data also suggest muscle-specific differences in NO-cGMP signaling supported by muscle-specific GC expression, GC activity, and GC agonist responsiveness. In addition, our data provide an important new understanding of the regulation of GC activity by nNOS. We show that GC complexes with nNOSμ and associates with a subset of nNOS splice variant compartments at the Golgi complex and neuromuscular junction, thus providing compelling evidence that differential GC NO receptor targeting could facilitate NO-cGMP signaling diversity in skeletal muscle. We advance understanding of the role of NO-cGMP signaling in mitochondrial biology by showing that GC1 is dispensable for mitochondrial content and function and that PDE5 is a negative regulator of mitochondrial ATP synthesis efficiency. These findings suggest a novel role for NO-cGMP-PDE5 signaling in skeletal muscle mitochondrial bioenergetics.

Skeletal muscle-specific differences in nNOSμ have been reported with glycolytic muscles exhibiting higher nNOSμ expression and NOS activity than oxidative muscles (41). In contrast, we find higher GC1 subunit expression in oxidative compared with glycolytic muscles, suggesting a general reciprocal relationship between nNOSμ and GC1 in skeletal muscles, that is, where nNOSμ expression is highest, GC1 is lowest. Higher relative GC1 expression in oxidative muscles suggests not only a larger cGMP-synthesizing capacity but also different responses to NO or cGMP modulation in these muscle types. Supporting this possibility, treating the mdx mouse model of DMD with sildenafil reduced dystrophic diaphragm muscle dysfunction with no impact on the TA (60).

Evidence of a close functional relationship between GC and nNOS was supported by immunoprecipitation and subcellular localization studies. α1GC and nNOSμ were found together in a cytoplasmic complex. Subcellular localization analyses show that α1GC and β1GC associated with the *cis*-Golgi complex. These data support an association of GC1 with the Golgi complex and suggest a role for NO-cGMP signaling in the secretory or endocrine functions of skeletal muscle. In addition, we found that unlike nNOSμ, GC was not localized to the sarcolemma, strengthening the case that GC does not target to the sarcolemma (23, 28). We also found that β1GC was enriched at the neuromuscular junction where α1GC, nNOSμ, and cGMP-dependent protein kinase localization were previously found (2, 16, 23). The functions of NO-cGMP signaling at the neuromuscular synapse remain unclear, but current evidence argues against a major role for synaptic nNOS in AchR distribution or neuromuscular transmission, but a possible role in agrin signaling (Supplementary Fig. S1G) (1, 29). Thus, GC at the neuromuscular junction may similarly be involved in agrin signaling. The findings suggest that restricting the localization of GC to the Golgi and neuromuscular junction could act as a mechanism to generate functional differences in NO signal transduction between these sites.

Additional evidence of a strong functional relationship between GC and nNOS came from the findings that baseline GC activity and GC responsiveness to NO donor, GC stimulator, or GC activator agonists were nNOS dependent. Our GC activity studies provided two noteworthy findings. First,

FIG. 8. PDE5 negatively modulates skeletal muscle mitochondrial ATP synthesis efficiency and capacity without impacting mitochondrial content. Skeletal muscle mitochondrial function was measured by *in vivo* spectroscopy in WT mice treated with sildenafil for 3 months to increase cGMP. **(A)** Mitochondrial ATP synthesis efficiency as measured by the P/O ratio. **(B)** Mitochondrial ATP synthesis rate (which is directly proportional to ATPase activity). **(C)** Mitochondrial oxygen consumption rate. For **(A–C)**, $n=7$ and 6 for untreated WT and sildenafil-treated groups, respectively. **(D)** Mitochondrial ATP synthesis capacity (ATPmax). $n=6$ for both groups. **(E)** Phosphocreatine (PCr)-to-ATP metabolite ratio. **(F)** Hind limb muscle phosphocreatine metabolite levels. **(G)** Hind limb muscle ATP levels. For **(E–G)**, $n=7$ and 6 for untreated WT and sildenafil-treated groups, respectively. **(H)** Densitometric quantitation of Western blots of mitochondrial marker VDAC1 protein expression in TA muscles. **(I)** Densitometric quantitation of Western blots of mitochondrial respiratory complex subunit expression in TA muscles. For **(H, I)**, $n=7$ and 4 for untreated WT and sildenafil-treated groups, respectively. **(J)** Quantitation of IFM volume density by electron microscopy-based stereology. **(K)** Electron microscopy-based quantitation of subsarcolemmal mitochondria density in TA muscles. For **(J, K)**, $n=3$–4 for each group. **(L)** Immunoassay-based quantitation of cGMP concentrations in gastrocnemius muscles from WT and sildenafil-treated mice ($n=7$ and 6, respectively). $^*p<0.05$; $^{**}p<0.01$, by Student's unpaired *t*-test comparison between untreated and sildenafil-treated mice. IFM, intermyofibrillar mitochondria.

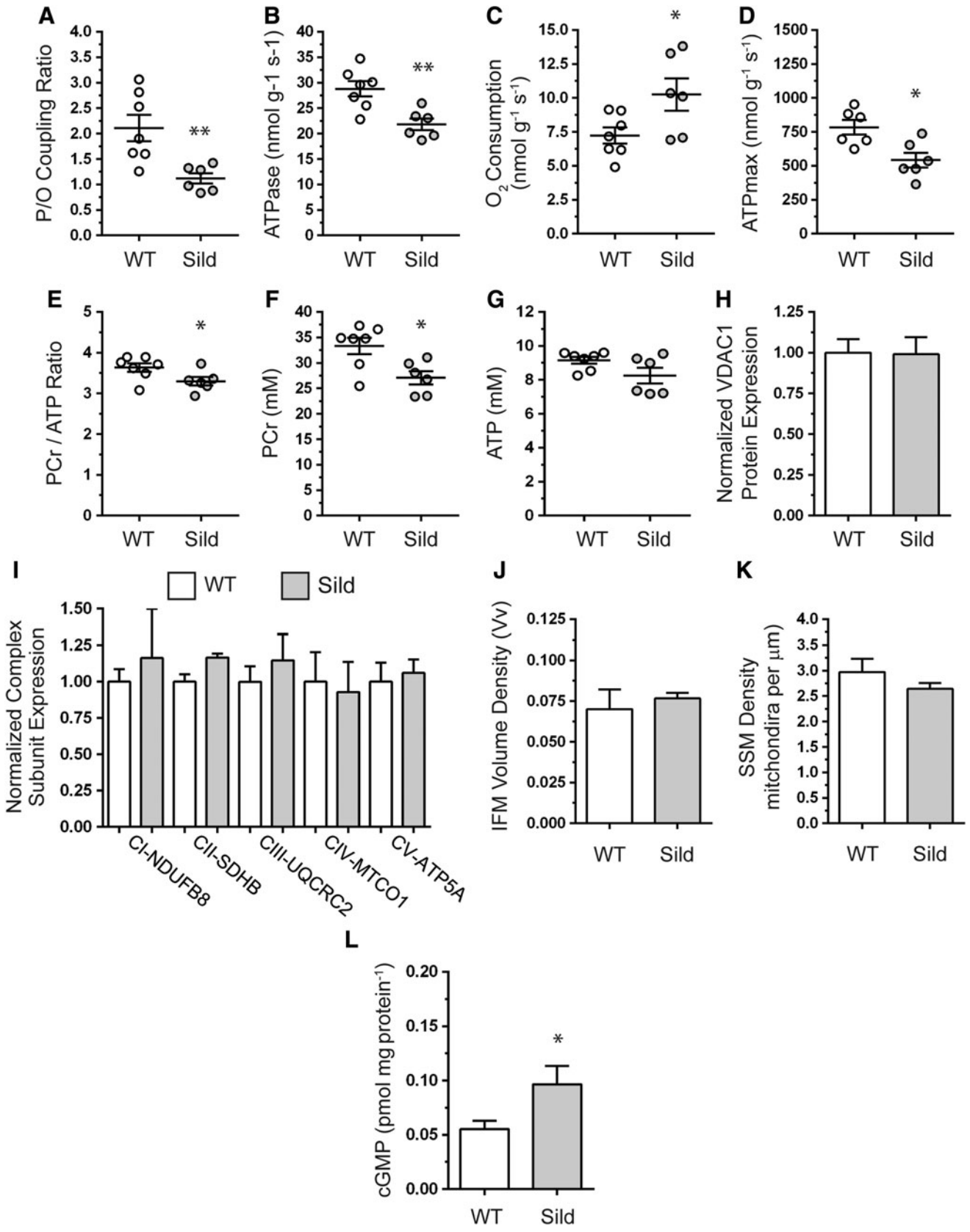
A
P/O Coupling Ratio
WT
Sild
B
ATPase (nmol g-1 s-1)
C
O2 Consumption (nmol g-1 s-1)
D
ATPmax (nmol g-1 s-1)
E
PCr / ATP Ratio
F
PCr (mM)
G
ATP (mM)
H
Normalized VDAC1 Protein Expression
I
Normalized Complex Subunit Expression
CI-NDUFB8
CII-SDHB
CIII-UQCRC2
CIV-MTCO1
CV-ATP5A
J
IFM Volume Density (Vv)
K
SSM Density mitchondira per μm)
L
cGMP (pmol mg protein-1)

the GC stimulator, BAY 41-2722, exhibited nNOS dependence in the TA, which was surprising since its action is widely considered NO independent. However, BAY 41-2722 did raise GC activity to wild-type levels in the soleus, suggesting muscle-specific differences in BAY 41-2722 action. Second, addition of DETANO could not activate GC to wild-type levels in the absence of nNOS. This suggested the remarkable possibility that exogenous NO could not fully recapitulate the GC-activating function of endogenous nNOS-derived NO for reasons that remain to be deciphered. Our data suggest that nNOS is an important determinant of GC activity, providing new mechanistic understanding of the regulation of GC and supporting GC1 as an important target of nNOS.

Analyses of muscle contractility in $GC1^{-/-}$ mice suggested that GC1 was dispensable for muscle strength since specific force was normal. This contrasts with early studies suggesting that NO and cGMP promote skeletal muscle weakness (41, 62). However, subsequent studies by the same group made the opposite conclusion that NO in fact promotes muscle contractility under physiological conditions (20, 32). This reevaluation agrees with the majority of subsequent studies, including the present one, which provides new evidence that NO-cGMP signaling does not inhibit muscle strength (54, 56).

While GC1 was dispensable for muscle strength, it was essential for normal fatigue resistance and force recovery after a fatiguing protocol. The extent of fatigue in $GC^{-/-}$ muscles was comparable in magnitude with that in $nNOS\mu^{-/-}$ muscles, but not in $nNOS\mu/\beta^{-/-}$ muscles, which exhibited greater fatigability (57). This may suggest a more important role for $\alpha2\beta1$ sGC or NO-driven S-nitrosylation in skeletal muscle fatigue resistance. In addition, it is important to note that we cannot rule out potential compensatory increases in $\alpha2\beta1$ sGC resting activity or $\alpha2\beta1$ sGC responsiveness to agonist stimulation that occurs without a change in $\alpha2\beta1$ sGC expression**.** Nonetheless, our finding suggests that NO signaling through GC1 is necessary for normal muscle fatigue resistance under physiological conditions. This new insight into the role of NO-GC-cGMP signaling in muscle fatigue has potential implications for understanding poor fatigue resistance and an exaggerated fatigue response to mild exercise in DBMD patients whose muscles have low nNOS and GC activities (10, 13, 40). Our data suggest that defective NO-GC signaling may exacerbate contraction-induced fatigue and postexercise muscle weakness in DBMD patients.

While changes in fiber type were an unlikely cause of muscle fatigue in $GC1^{-/-}$ mice, our data did provide new evidence that NO plays an important role in regulating muscle fiber type partly through a GC1-dependent mechanism. $GC1^{-/-}$ males exhibited a type IIA to IIX fiber-type shift. Importantly, $nNOS\mu$ was shown to negatively regulate type IIX fiber composition, although sex was not included as a variable in this study (57). Thus, $nNOS\mu$ may regulate muscle type IIX fiber content through a sex-specific and GC1-dependent mechanism. Taken together, these data suggest that nNOS promotes muscle fatigue resistance partly through a GC1-dependent, but fiber-type-independent, mechanism.

In addition to regulating fiber type, GC1 may also regulate the organization of the subsarcolemmal microtubule cytoskeleton. $GC1^{-/-}$ muscles exhibited a qualitative and quantitative disruption of the microtubule lattice intermediate in severity between wild-type and $nNOS^{-/-}$ muscle, consistent with our report of a qualitative disruption of subsarcolemmal microtubules in $nNOS^{-/-}$ muscles (57). Taken together, these findings suggest that nNOS may regulate subsarcolemmal microtubule organization, partly through GC1, and that NO-cGMP signaling is an important regulator of the microtubule cytoskeleton in skeletal muscle. This raises the question of what the consequences of microtubule disruption might be. Microtubules play firmly established roles in the scaffolding and dynamics of organelles, including the Golgi complex and mitochondria. Therefore, microtubule disorganization may contribute to aberrant Golgi complex localization and mitochondrial morphology in $nNOS^{-/-}$ muscles (57). However, Golgi localization was not impaired in $GC1^{-/-}$ muscles, possibly because Golgi localization is more dependent on longitudinal microtubules, which were better preserved in $GC1^{-/-}$ than $nNOS^{-/-}$ muscles. Microtubule defects in $GC1^{-/-}$ mice were also not associated with defects in mitochondrial ATP synthesis or content. However, microtubule defects were associated with increased fatigability and impaired postexercise force recovery in both $nNOS^{-/-}$ and $GC1^{-/-}$ muscles, as well as muscle weakness in $nNOS^{-/-}$ muscles (57). So, NO-cGMP pathways may regulate muscle contractile function, in part, through a microtubule-dependent mechanism.

Microtubule defects were not associated with defects in mitochondrial ATP synthesis or content in $GC1^{-/-}$ skeletal muscle, indicating that cGMP synthesis by GC1 is dispensable for mitochondrial ATP synthesis and content in resting muscle. However, blocking cGMP breakdown by PDE5 with sildenafil reduced ATP synthesis efficiency, with mitochondria consuming larger amounts of O_2 and substrates (*e.g.*, fatty acids and sugars) to generate ATP. While the mechanisms underpinning reduced ATP synthesis efficiency remain to be determined, proton and electron leaks from the electron transport chain represent an attractive causal mechanism (3). These findings support a novel role for PDE5 as a regulator of ATP synthesis efficiency and skeletal muscle bioenergetics.

NO has been previously linked to skeletal muscle mitochondrial ATP synthesis efficiency in humans (42). Dietary nitrate supplementation increased ATP synthesis efficiency in healthy humans by reducing proton leak without impacting biogenesis (42). In contrast, we find that increasing NO-cGMP signaling decreased ATP synthesis efficiency in healthy mice. However, both studies support a role for NO in modulating ATP synthesis efficiency. One other interesting result was that cGMP enhancement with sildenafil had no impact on total, subsarcolemmal, or intermyofibrillar mitochondrial content. This argues against compensatory biogenesis in the face of decreased efficiency and contrasts with reports showing that increases in NO or cGMP promote biogenesis (18, 43, 52, 53). It is conceivable that PDE5 does not regulate biogenesis in muscle or that sildenafil did not produce a sufficient cGMP increase to induce biogenesis. This is important because biogenesis may occur in response to high or supraphysiological increases in NO-cGMP signaling (49, 52, 53). Taken together, our data suggest that NO-cGMP-PDE5 signaling modulates mitochondrial ATP synthesis independently of mitochondrial content.

Strategies that partially uncouple skeletal muscle mitochondria to promote inefficiency represent an attractive antiobesity therapy for humans because they increase energy

expenditure and promote fat loss (33). Recent evidence suggests that decreased NO-cGMP signaling in tissues, including skeletal muscle, is a pathogenic feature of obesity (31, 39, 48, 49, 51). Enhancing NO-cGMP signaling in mouse models of diet-induced obesity with sildenafil, GC stimulator, BAY 41-8543, or by PKGI overexpression protected against high-fat diet-driven energy imbalance and insulin resistance (4, 7, 35, 36, 48, 49, 51). However, the mechanisms by which PDE5 inhibition protects against obesity remain unclear (37, 48). Based on our data, it is tempting to speculate that one novel mechanism by which PDE5 inhibition may protect against obesity is through induction of inefficient mitochondrial ATP synthesis in skeletal muscle, which would increase energy consumption and promote a negative energy balance.

Materials and Methods

Mouse models

Mice lacking nNOS activity ($nNOS^{-/-}$) were generated by targeted deletion of exon 6 of the *NOS1* gene and have been described previously (30). Mice lacking active guanylate cyclase 1 (GC1) were previously generated by targeted deletion of exon 6 encoding part of the catalytic domain of the α1 subunit of GC1 (11). GC1 mice express a truncated, but catalytically inactive, GC1. All mice were on congenic C57Bl backgrounds and age- and sex-matched adult littermates were used unless otherwise stated. Mice harboring mutations in members of nNOS-NO-GC-cGMP signal transduction pathways exhibit sex-specific cardiovascular, motor, and reproductive phenotypes; therefore, sex was considered as an experimental variable (11, 26, 30, 56, 69). Where sex-specific differences were observed, male and female data are reported separately. If no difference between sexes was observed, then the data were pooled. All experimental procedures performed on mice were approved by the Institutional Animal Care and Use Committees of the University of Miami.

Sildenafil administration

The PDE5 inhibitor sildenafil dosing regimen has been previously described where sildenafil citrate (Pfizer) was administered in the drinking water *ad libitum* (400 mg/L) to wild-type mice for 14 weeks starting after weaning (60).

Dual-energy X-ray absorptiometry densitometry

Body composition, including bone mineral density, and body fat percentage of 4-month-old mice were determined by dual-energy X-ray absorptiometry densitometry in Avertin-anesthetized mice using a Lunar PIXImus Densitometer (GE Medical Systems) according to the manufacturer's instructions.

Immunofluorescence labeling and confocal microscopy of myofibers

The methodology used to immunolabel single myofibers is identical to that previously reported, except that confocal images were captured with an Olympus FluoView FV1000 confocal microscope (58). Identical laser power, excitation, and emission capture settings were used when comparing β1GC localization between wild-type and $GC1^{-/-}$ muscles. Primary antibodies used were α1GC (Sigma-Aldrich), β1GC (Sigma-Aldrich), and α2GC (Thermo Scientific). FITC-conjugated anti-α tubulin antibodies were used to label microtubules (Sigma-Aldrich; clone DM1A). Acetylcholine receptors were labeled with Alexa 488-conjugated α-bungarotoxin (Invitrogen).

Western immunoblotting

Skeletal muscles were homogenized in buffer (2% sodium dodecyl sulfate, 50 m*M* Tris-HCl, pH 6.8) with protease and phosphatase inhibitors (Roche). Thirty micrograms of protein per sample was electrophoresed on 4–20% Mini-PROTEAN TGX Stain-Free Precast Gels (Bio-Rad) and transferred to polyvinylidene fluoride membranes (Millipore). Equivalency of loading in gels and membranes was determined using the stain-free detection system and a Bio-Rad Chemi-Doc MP imager. Protein expression was normalized to total transferred protein using Bio-Rad ImageLab 5.2.1 software. Membranes were blocked with 5% (w/v) skim milk in Tris-buffered saline with Tween-20 for 1 h at room temperature and incubated with primary antibodies overnight at 4°C. Primary antibodies used were rabbit anti-VDAC1 (Sigma Aldrich), rabbit pan anti-nNOS (Sigma-Aldrich), and rabbit anti-phospho $nNOS^{1412}$ (Abcam). ser1412 corresponds to ser1446 in nNOSμ due to the 34 amino acid μ insert (68). MitoProfile® total OXPHOS antibody cocktail (Abcam) was used to detect respiratory complex subunits NDUFB8 (Complex I or CI), SDHB (CII), UQCRC2 (CIII), MTCO1 (CIV), and ATP5A (CV). Primary antibodies were detected with donkey horseradish peroxidase-conjugated secondary antibodies (Jackson ImmunoResearch Laboratories). Chemiluminescence was visualized with SuperSignal West Femto Maximum Sensitivity substrate (Thermo Fisher) on a Biorad ChemiDoc MP imaging system.

Soluble guanylate cyclase activity

Soluble guanylate cyclase (GC) enzyme activity in skeletal muscles was measured as described (11). Briefly, muscles were homogenized in buffer containing 50 m*M* Tris-HCl (pH 7.6), 1 m*M* EDTA, 1 m*M* dithiothreitol, and 2 m*M* phenylmethylsulfonyl fluoride. Extracts were centrifuged at 20,000 *g* for 20 min at 4°C. Supernatants containing 50 μg protein were incubated for 10 min at 37°C with 50 m*M* Tris-HCl (pH 7.5), 4 m*M* $MgCl_2$, 0.5 m*M* 1-methyl-3-isobutylxanthine, 7.5 m*M* creatine phosphate, 0.2 mg/ml creatine phosphokinase, 1 m*M* L-NAME, and 1 m*M* GTP with or without 10 μ*M* of NO donor, DETANO, 100 μ*M* sGC activator, BAY 58-2667 (cinaciguat), or 1 m*M* of sGC stimulator, BAY 41-2272 (22, 24, 70). BAY 58-2667 activates GC only when it is oxidized (Fe^{3+}) or in a heme-free state, providing additive, but not synergistic, effects with NO, which cannot activate GC in this state. Thus, BAY 58-2667 GC activator is an NO- and heme-independent agonist. BAY 41-2272 is an NO-independent allosteric GC stimulator that binds the reduced (Fe^{2+}) form of GC, making it sensitive to low NO concentrations. BAY 41-2272 is considered an NO-independent and heme-dependent GC agonist. The reaction was terminated with 0.05 *M* HCl. cGMP was measured by immunoassay (Cayman Chemical). sGC activity was expressed as picomoles of cGMP synthesized per milligram of muscle protein per minute.

Immunoprecipitation assays

Skeletal muscle tissues were lysed in buffer containing 1% Nonidet P-40, 50 m*M* Tris-HCL, pH 7.4, 150 m*M* NaCl, 2 m*M* EGTA, 2 m*M* PMSF, and protease inhibitor cocktail (Roche Applied Science). Immunoprecipitations were performed using the Dynabeads® Protein G immunoprecipitation kit (Invitrogen) according to the manufacturer's instructions using an anti-α1 sGC (GC1) antibody (Sigma-Aldrich). Bound protein was eluted in loading buffer containing 1% SDS. Sample lysates were then analyzed by Western blot using an anti-nNOS antibody (BD Biosciences).

Analyses of muscle histopathology, central nucleation, fiber type, and myofiber area

Freshly isolated skeletal muscles were flash-frozen in liquid nitrogen-cooled 2-methylbutane. Ten-micron-thick cryosections cut from muscle mid-bellies were stained with hematoxylin and eosin using standard methods. Muscles were inspected for evidence of myopathy or dystrophy marked by occurrence of central nucleation, increased fiber size heterogeneity, and immune cell infiltration as described (27, 57, 60). Immunofluorescent labeling of transverse muscle cryosections was performed as previously described (27). To discern shifts in fiber composition, muscle mid-belly cryosections were immunolabeled with a cocktail of monoclonal antibodies against type I (clone BA-D5), type IIA (clone SC-71), and type IIB (clone BF-F3) myosin heavy chains (Developmental Studies Hybridoma Bank) as described (57). Antimyosin antibodies were detected using isotype-specific secondary antibodies: Alexa Fluor 350-labeled donkey anti-mouse IgG2B (BA-D5), Alexa Fluor 594-labeled donkey anti-mouse IgG1 (SC-71), and Alexa Fluor 488 donkey anti-mouse IgM (BF-F3). The incidence (number of positive muscle cells divided by the total number of muscle cells in the entire section) of type I, type IIA, and type IIB myosin heavy chain-positive muscle cells was determined manually. Unlabeled fibers were designated type IIX. Feret diameters and cross-sectional areas of 300 type IIX myofibers, 400 type IIB, and 100 type IIA myofibers, representing about a quarter of each myofiber fiber type, were determined per mouse from spatially calibrated images using ImageJ 1.46r software (64).

Automated bright-field and immunofluorescence microscopy

For microscopic analyses of muscle morphology and fiber type, images of entire muscle sections were obtained at 20$\times$magnification with a DP80 digital camera (Olympus) in combination with an automated capture and tiling system. The system was run by CellSens software (Olympus) and comprised an Olympus BX50 upright microscope fitted with a Prior Scientific motorized x-y stage. Images of whole muscle sections labeled with hematoxylin and eosin were created by stitching individual color images captured sequentially together into a single composite image. For fluorescent images obtained in fiber typing experiments, individual images of Alexa 350, 488, and 594 fluorescence emissions were captured sequentially, then automatically stitched together to form a composite image of the entire muscle cross section.

Gene expression analysis

PGC1α, Atrogin 1, and MuRF1 transcript expression levels were determined by quantitative real-time PCR. Total RNA was isolated from skeletal muscles using TRIzol reagent (Invitrogen) according to the manufacturer's instructions. cDNAs were generated from 1 μg of total RNA using the iScript™ cDNA Synthesis Kit (Bio-Rad). Real-time PCR was performed using the Sso Advanced Universal SYBR Green Supermix (Bio-Rad) on CFX Connect Real-Time PCR detection system (Bio-Rad). Gene expression was normalized to the Rps18 housekeeping gene and analyzed using the $\Delta\Delta C_T$ method with Bio-Rad CFX Manager 3.1 software (45). Atrogin 1 forward and reverse primer sequences are 5′-AAAGGG CAGCTGGATTGGAA and 5′-TGAGGGGAAA-GTGAGA CGGA, respectively. MuRF1 forward and reverse primer sequences are 5′-GTCTG-GAGGTCGTTTCCGTT and 5′-AG CAAGTAGGCACCTCACAC, respectively. PGC1α primers were purchased from Biorad (qMmuCID0006032).

Quantitation of microtubule directionality and density

Microtubule directionality measurements were made using texture detection (TedT) software (44). Confocal images representing either a single optical section or a maximum projection of 1–3 sections containing the subsarcolemmal microtubule cytoskeleton were captured. Images were automatically contrasted and rotated using Adobe Photoshop software so that the long axis of the myofiber ran from left to right. Images were opened in (TedT) software, two peaks and two valleys were selected, and then general directionality scores (D), vertical directionality scores (D_V), and directionality histograms (H_D) were determined. Texture correlation values for individual images were normalized and plotted against microtubule orientation. Subsarcolemmal microtubule densities in single myofibers were captured by thresholding tubulin fluorescence at different gray values from 8-bit grayscale images using ImageJ version 1.46r software. The number of tubulin-positive pixels and total number of pixels in the myofiber were determined using the histogram algorithm in ImageJ. The fraction of tubulin-positive pixels was normalized to the mean control value. For all analyses, microtubules associated with nonmuscle cells and myonuclei were excluded; 14–18 representative images from at least three mice per group were analyzed.

In situ *measurement of TA strength and fatigue resistance*

Tests of muscle contractile performance were performed on the TA muscle *in situ* in anesthetized mice as described (56). The contractile function of the TA muscle was measured using an *in situ* muscle test system (Aurora Scientific, Inc.) Briefly, anesthetized mice were positioned on a heated platform and the distal tendon of the TA was attached to the lever arm of a servomotor. The TA muscle was activated by peroneal nerve stimulation using needle electrodes and adjusted to an optimum length (L_o) to produce the maximum tetanic force. Specific force was determined by normalizing force output to muscle cross-sectional area ($L_o\times$pennation angle correction factor$\times$density]/muscle mass). To test the susceptibility of muscles to fatiguing stimulation, TA muscles were subjected to fatigue protocol of 120 isometric

tetanic stimulations (200 Hz) at 2-s intervals lasting 4 min. Following the fatigue protocol, force output was determined after 1, 3, and 5 min to monitor the muscle force recovery.

In vivo *metabolic spectroscopy analysis of mitochondrial ATP synthesis*

These methods have been described in detail previously (59, 65, 67). Briefly, muscles of the lower hind limbs of anesthetized mice were subject to a short bout of ischemia, and then allowed to recover. Fluxes in muscle mitochondrial ATP generation and O_2 consumption were simultaneously measured during ischemia and recovery periods by ^{31}P magnetic resonance and optical spectroscopy, respectively (5, 67). These fluxes were used to calculate the efficiency of mitochondrial ATP synthesis (P/O coupling ratio) and maximal ATP synthesis capacity. Mice were anesthetized with intraperitoneal injections of 0.01 ml g^{-1} of 2.5% tribromoethanol (Sigma-Aldrich), then strapped into a custom-built multimode probe for ^{31}P magnetic resonance and optical spectroscopy developed for a 7T vertical bore spectrometer (Varian). Following signal optimization, ^{31}P and optical spectra were collected concurrently during an initial resting period ($\sim$2 min), then during hind limb ischemia ($\sim$11 min) and recovery ($\sim$7 min) periods. The resulting ^{31}P and optical spectra were processed as described previously and were used to derive resting rates of mitochondrial ATP production (ATPase, P) and O_2 consumption (O), efficiency of coupling of oxidation to phosphorylation (P/O), and the maximum rate of oxidative phosphorylation (ATPmax) (59, 65, 66). ATP, PCr, hemoglobin, and myoglobin concentrations were quantitated from pooled hind limb skeletal muscles as described previously (46).

Quantitation of mitochondrial content by transmission electron microscopy

Mitochondrial ultrastructure, subsarcolemmal, and intermyofibrillar mitochondrial pool densities were determined in TA muscles by transmission electron microscopy analysis as described previously (57, 59).

cGMP quantitation

Acetylated cGMP levels in skeletal muscle lysates were quantitated by Detect X® Direct Cyclic GMP immunoassay according to the manufacturer's instructions (Arbor Assays). Optical densities were read at 450 nm with a Synergy H1 microplate reader using Gen5 Imager Software (BioTek Instruments, Inc.) cGMP was normalized to protein concentrations determined with a Pierce™ BCA Protein Assay Kit with BSA as standard (Thermo Fisher Scientific). All assays were in duplicate, and cGMP concentrations expressed as picomoles per milligram of protein.

Statistical analyses

All values are reported as mean ± standard error of the mean. Protein and mRNA expression data were normalized by dividing all values by the mean of the wild-type control group. The specific statistical tests used to determine significant differences between group means are included in figure legends. Statistical calculations were performed using Prism v 6.07 (Graphpad Software, Inc.), with p values <0.05 considered significant.

Acknowledgments

This research was funded by NIH RC2 AG036606 (D.J.M.). The authors thank Dr Wenhua Liu from the Light Image Section of National Institute of Arthritis and Musculoskeletal and Skin Disease at the National Institutes of Health for generously providing the TeDT software. The authors also thank Dr. Kimberley Craven for critically editing the manuscript.

Author Disclosure Statement

Dr. Percival has a consultancy relationship with Ironwood Pharmaceuticals and has received material support from Bayer Pharma. The coauthors report no potential conflicts.

References

1. Adams ME, Kramarcy N, Fukuda T, Engel AG, Sealock R, and Froehner SC. Structural abnormalities at neuromuscular synapses lacking multiple syntrophin isoforms. *J Neurosci* 24: 10302–10309, 2004.
2. Adams ME, Kramarcy N, Krall SP, Rossi SG, Rotundo RL, Sealock R, and Froehner SC. Absence of alpha-syntrophin leads to structurally aberrant neuromuscular synapses deficient in utrophin. *J Cell Biol* 150: 1385–1398, 2000.
3. Affourtit C, Quinlan CL, and Brand MD. Measurement of proton leak and electron leak in isolated mitochondria. *Methods Mol Biol* 810: 165–182, 2012.
4. Al-biati HA, Ismail SH, Sahib AS, Kazaal FAK, and Al-Rubaie S. Effects of sildenafil on lipid profile and glycemic control in patients with type 2 diabetes mellitus and metabolic syndrome. *Int J Basic Clin Pharmacol* 3: 1048–1051, 2014.
5. Amara CE, Marcinek DJ, Shankland EG, Schenkman KA, Arakaki LS, and Conley KE. Mitochondrial function in vivo: spectroscopy provides window on cellular energetics. *Methods* 46: 312–318, 2008.
6. Asai A, Sahani N, Kaneki M, Ouchi Y, Martyn JA, and Yasuhara SE. Primary role of functional ischemia, quantitative evidence for the two-hit mechanism, and phosphodiesterase-5 inhibitor therapy in mouse muscular dystrophy. *PLoS One* 2: e806, 2007.
7. Ayala JE, Bracy DP, Julien BM, Rottman JN, Fueger PT, and Wasserman DH. Chronic treatment with sildenafil improves energy balance and insulin action in high fat-fed conscious mice. *Diabetes* 56: 1025–1033, 2007.
8. Bassel-Duby R and Olson EN. Signaling pathways in skeletal muscle remodeling. *Annu Rev Biochem* 75: 19–37, 2006.
9. Bloom TJ. Cyclic nucleotide phosphodiesterase isozymes expressed in mouse skeletal muscle. *Can J Physiol Pharmacol* 80: 1132–1135, 2002.
10. Brenman JE, Chao DS, Xia H, Aldape K, and Bredt DS. Nitric oxide synthase complexed with dystrophin and absent from skeletal muscle sarcolemma in Duchenne muscular dystrophy. *Cell* 82: 743–752, 1995.
11. Buys ES, Sips P, Vermeersch P, Raher MJ, Rogge E, Ichinose F, Dewerchin M, Bloch KD, Janssens S, and Brouckaert P. Gender-specific hypertension and responsiveness to nitric oxide in sGCalpha1 knockout mice. *Cardiovasc Res* 79: 179–186, 2008.
12. Cawley SM, Kolodziej S, Ichinose F, Brouckaert P, Buys ES, and Bloch KD. sGC{alpha}1 mediates the negative inotropic effects of NO in cardiac myocytes independent of changes in calcium handling. *Am J Physiol Heart Circ Physiol* 301: H157–H163, 2011.

13. Cerri C, Canal N, and Frattola L. Guanylate cyclase activity in normal and diseased human muscle. *J Neurol Neurosurg Psychiatry* 41: 805–808, 1978.
14. Chang WJ, Iannaccone ST, Lau KS, Masters BS, McCabe TJ, McMillan K, Padre RC, Spencer MJ, Tidball JG, and Stull JT. Neuronal nitric oxide synthase and dystrophin-deficient muscular dystrophy. *Proc Natl Acad Sci U S A* 93: 9142–9147, 1996.
15. Chao DS, Gorospe JR, Brenman JE, Rafael JA, Peters MF, Froehner SC, Hoffman EP, Chamberlain JS, and Bredt DS. Selective loss of sarcolemmal nitric oxide synthase in Becker muscular dystrophy. *J Exp Med* 184: 609–618, 1996.
16. Chao DS, Silvagno F, Xia H, Cornwell TL, Lincoln TM, and Bredt DS. Nitric oxide synthase and cyclic GMP-dependent protein kinase concentrated at the neuromuscular endplate. *Neuroscience* 76: 665–672, 1997.
17. De Palma C, Falcone S, Pisoni S, Cipolat S, Panzeri C, Pambianco S, Pisconti A, Allevi R, Bassi MT, Cossu G, Pozzan T, Moncada S, Scorrano L, Brunelli S, and Clementi E. Nitric oxide inhibition of Drp1-mediated mitochondrial fission is critical for myogenic differentiation. *Cell Death Differ* 17: 1684–1696, 2010.
18. De Palma C, Morisi F, Pambianco S, Assi E, Touvier T, Russo S, Perrotta C, Romanello V, Carnio S, Cappello V, Pellegrino P, Moscheni C, Bassi MT, Sandri M, Cervia D, and Clementi E. Deficient nitric oxide signalling impairs skeletal muscle growth and performance: involvement of mitochondrial dysregulation. *Skelet Muscle* 4: 22, 2014.
19. Derbyshire ER and Marletta MA. Structure and regulation of soluble guanylate cyclase. *Annu Rev Biochem* 81: 533–559, 2012.
20. Eu JP, Hare JM, Hess DT, Skaf M, Sun J, Cardenas-Navina I, Sun QA, Dewhirst M, Meissner G, and Stamler JS. Concerted regulation of skeletal muscle contractility by oxygen tension and endogenous nitric oxide. *Proc Natl Acad Sci U S A* 100: 15229–15234, 2003.
21. Eu JP, Sun J, Xu L, Stamler JS, and Meissner G. The skeletal muscle calcium release channel: coupled O2 sensor and NO signaling functions. *Cell* 102: 499–509, 2000.
22. Evgenov OV, Pacher P, Schmidt PM, Hasko G, Schmidt HH, and Stasch JP. NO-independent stimulators and activators of soluble guanylate cyclase: discovery and therapeutic potential. *Nat Rev Drug Discov* 5: 755–768, 2006.
23. Feussner M, Richter H, Baum O, and Gossrau R. Association of soluble guanylate cyclase with the sarcolemma of mammalian skeletal muscle fibers. *Acta Histochem* 103: 265–277, 2001.
24. Follmann M, Griebenow N, Hahn MG, Hartung I, Mais FJ, Mittendorf J, Schafer M, Schirok H, Stasch JP, Stoll F, and Straub A. The chemistry and biology of soluble guanylate cyclase stimulators and activators. *Angew Chem Int Ed Engl* 52: 9442–9462, 2013.
25. Francis SH, Blount MA, and Corbin JD. Mammalian cyclic nucleotide phosphodiesterases: molecular mechanisms and physiological functions. *Physiol Rev* 91: 651–690, 2011.
26. Friebe A and Koesling D. The function of NO-sensitive guanylyl cyclase: what we can learn from genetic mouse models. *Nitric Oxide* 21: 149–156, 2009.
27. Froehner SC, Reed SM, Anderson KN, Huang PL, and Percival JM. Loss of nNOS inhibits compensatory muscle hypertrophy and exacerbates inflammation and eccentric contraction-induced damage in mdx mice. *Hum Mol Genet* 24: 492–505, 2014.
28. Fukutani T, Iino S, and Nojyo Y. The expression of soluble guanylate cyclase in the vasculature of rat skeletal muscle. *Arch Histol Cytol* 72: 117–126, 2009.
29. Godfrey EW, Longacher M, Neiswender H, Schwarte RC, and Browning DD. Guanylate cyclase and cyclic GMP-dependent protein kinase regulate agrin signaling at the developing neuromuscular junction. *Dev Biol* 307: 195–201, 2007.
30. Gyurko R, Leupen S, and Huang PL. Deletion of exon 6 of the neuronal nitric oxide synthase gene in mice results in hypogonadism and infertility. *Endocrinology* 143: 2767–2774, 2002.
31. Haas B, Mayer P, Jennissen K, Scholz D, Berriel Diaz M, Bloch W, Herzig S, Fassler R, and Pfeifer A. Protein kinase G controls brown fat cell differentiation and mitochondrial biogenesis. *Sci Signal* 2: ra78, 2009.
32. Haldar SM and Stamler JS. S-nitrosylation: integrator of cardiovascular performance and oxygen delivery. *J Clin Invest* 123: 101–110, 2013.
33. Harper ME, Green K, and Brand MD. The efficiency of cellular energy transduction and its implications for obesity. *Annu Rev Nutr* 28: 13–33, 2008.
34. Hinchee-Rodriguez K, Garg N, Venkatakrishnan P, Roman MG, Adamo ML, Masters BS, and Roman LJ. Neuronal nitric oxide synthase is phosphorylated in response to insulin stimulation in skeletal muscle. *Biochem Biophys Res Commun* 435: 501–505, 2013.
35. Ho JE, Arora P, Walford GA, Ghorbani A, Guanaga DP, Dhakal BP, Nathan DI, Buys ES, Florez JC, Newton-Cheh C, Lewis GD, and Wang TJ. Effect of phosphodiesterase inhibition on insulin resistance in obese individuals. *J Am Heart Assoc* 3: e001001, 2014.
36. Hoffmann LS, Etzrodt J, Willkomm L, Sanyal A, Scheja L, Fischer AW, Stasch JP, Bloch W, Friebe A, Heeren J, and Pfeifer A. Stimulation of soluble guanylyl cyclase protects against obesity by recruiting brown adipose tissue. *Nat Commun* 6: 7235, 2015.
37. This reference has been deleted.
38. Ito N, Ruegg UT, Kudo A, Miyagoe-Suzuki Y, and Takeda S. Activation of calcium signaling through Trpv1 by nNOS and peroxynitrite as a key trigger of skeletal muscle hypertrophy. *Nat Med* 19: 101–106, 2013.
39. Kim GW, Lin JE, Blomain ES, and Waldman SA. Antiobesity pharmacotherapy: new drugs and emerging targets. *Clin Pharmacol Ther* 95: 53–66, 2014.
40. Kobayashi YM, Rader EP, Crawford RW, Iyengar NK, Thedens DR, Faulkner JA, Parikh SV, Weiss RM, Chamberlain JS, Moore SA, and Campbell KP. Sarcolemma-localized nNOS is required to maintain activity after mild exercise. *Nature* 456: 511–515, 2008.
41. Kobzik L, Reid MB, Bredt DS, and Stamler JS. Nitric oxide in skeletal muscle. *Nature* 372: 546–548, 1994.
42. Larsen FJ, Schiffer TA, Borniquel S, Sahlin K, Ekblom B, Lundberg JO, and Weitzberg E. Dietary inorganic nitrate improves mitochondrial efficiency in humans. *Cell Metab* 13: 149–159, 2011.
43. Lira VA, Brown DL, Lira AK, Kavazis AN, Soltow QA, Zeanah EH, and Criswell DS. Nitric oxide and AMPK cooperatively regulate PGC-1 in skeletal muscle cells. *J Physiol* 588: 3551–3566, 2010.
44. Liu W and Ralston E. A new directionality tool for assessing microtubule pattern alterations. *Cytoskeleton (Hoboken)* 71: 230–240, 2014.
45. Livak KJ and Schmittgen TD. Analysis of relative gene expression data using real-time quantitative PCR and the 2(-Delta Delta C(T)) Method. *Methods* 25: 402–408, 2001.

46. Marcinek DJ, Schenkman KA, Ciesielski WA, and Conley KE. Mitochondrial coupling in vivo in mouse skeletal muscle. *Am J Physiol Cell Physiol* 286: C457–C463, 2004.
47. Martin EA, Barresi R, Byrne BJ, Tsimerinov EI, Scott BL, Walker AE, Gurudevan SV, Anene F, Elashoff RM, Thomas GD, and Victor RG. Tadalafil alleviates muscle ischemia in patients with Becker muscular dystrophy. *Sci Transl Med* 4: 162ra155, 2012.
48. Mitschke MM, Hoffmann LS, Gnad T, Scholz D, Kruithoff K, Mayer P, Haas B, Sassmann A, Pfeifer A, and Kilic A. Increased cGMP promotes healthy expansion and browning of white adipose tissue. *FASEB J* 27: 1621–1630, 2013.
49. Miyashita K, Itoh H, Tsujimoto H, Tamura N, Fukunaga Y, Sone M, Yamahara K, Taura D, Inuzuka M, Sonoyama T, and Nakao K. Natriuretic peptides/cGMP/cGMP-dependent protein kinase cascades promote muscle mitochondrial biogenesis and prevent obesity. *Diabetes* 58: 2880–2892, 2009.
50. Nelson MD, Rader F, Tang X, Tavyev J, Nelson SF, Miceli MC, Elashoff RM, Sweeney HL, and Victor RG. PDE5 inhibition alleviates functional muscle ischemia in boys with Duchenne muscular dystrophy. *Neurology* 82: 2085–2091, 2014.
51. Nikolic DM, Li Y, Liu S, and Wang S. Overexpression of constitutively active PKG-I protects female, but not male mice from diet-induced obesity. *Obesity (Silver Spring)* 19: 784–791, 2011.
52. Nisoli E, Clementi E, Paolucci C, Cozzi V, Tonello C, Sciorati C, Bracale R, Valerio A, Francolini M, Moncada S, and Carruba MO. Mitochondrial biogenesis in mammals: the role of endogenous nitric oxide. *Science* 299: 896–899, 2003.
53. Nisoli E, Falcone S, Tonello C, Cozzi V, Palomba L, Fiorani M, Pisconti A, Brunelli S, Cardile A, Francolini M, Cantoni O, Carruba MO, Moncada S, and Clementi E. Mitochondrial biogenesis by NO yields functionally active mitochondria in mammals. *Proc Natl Acad Sci U S A* 101: 16507–16512, 2004.
54. Percival JM. nNOS regulation of skeletal muscle fatigue and exercise performance. *Biophys Revi* 3: 209–217, 2011.
55. Percival JM, Adamo CM, Beavo JA, and Froehner SC. Evaluation of the therapeutic utility of phosphodiesterase 5A inhibition in the mdx mouse model of duchenne muscular dystrophy. *Handb Exp Pharmacol* 204: 323–344, 2011.
56. Percival JM, Anderson KN, Gregorevic P, Chamberlain JS, and Froehner SC. Functional deficits in nNOSmu-deficient skeletal muscle: myopathy in nNOS knockout mice. *PLoS One* 3: e3387, 2008.
57. Percival JM, Anderson KN, Huang P, Adams ME, and Froehner SC. Golgi and sarcolemmal neuronal NOS differentially regulate contraction-induced fatigue and vasoconstriction in exercising mouse skeletal muscle. *J Clin Invest* 120: 816–826, 2010.
58. Percival JM, Gregorevic P, Odom GL, Banks GB, Chamberlain JS, and Froehner SC. rAAV6-microdystrophin rescues aberrant Golgi complex organization in mdx skeletal muscles. *Traffic* 8: 1424–1439, 2007.
59. Percival JM, Siegel MP, Knowels G, and Marcinek DJ. Defects in mitochondrial localization and ATP synthesis in the mdx mouse model of Duchenne muscular dystrophy are not alleviated by PDE5 inhibition. *Hum Mol Genet* 22: 153–167, 2013.
60. Percival JM, Whitehead NP, Adams ME, Adamo CM, Beavo JA, and Froehner SC. Sildenafil reduces respiratory muscle weakness and fibrosis in the mdx mouse model of Duchenne muscular dystrophy. *J Pathol* 228: 77–87, 2012.
61. Rameau GA, Tukey DS, Garcin-Hosfield ED, Titcombe RF, Misra C, Khatri L, Getzoff ED, and Ziff EB. Biphasic coupling of neuronal nitric oxide synthase phosphorylation to the NMDA receptor regulates AMPA receptor trafficking and neuronal cell death. *J Neurosci* 27: 3445–3455, 2007.
62. Reid MB, Kobzik L, Bredt DS, and Stamler JS. Nitric oxide modulates excitation-contraction coupling in the diaphragm. *Comp Biochem Physiol A Mol Integr Physiol* 119: 211–218, 1998.
63. Schiaffino S and Reggiani C. Fiber types in mammalian skeletal muscles. *Physiol Rev* 91: 1447–1531, 2011.
64. Schneider CA, Rasband WS, and Eliceiri KW. NIH Image to ImageJ: 25 years of image analysis. *Nat Methods* 9: 671–675, 2012.
65. Siegel MP, Kruse SE, Knowels G, Salmon A, Beyer R, Xie H, Van Remmen H, Smith SR, and Marcinek DJ. Reduced coupling of oxidative phosphorylation in vivo precedes electron transport chain defects due to mild oxidative stress in mice. *PLoS One* 6: e26963, 2011.
66. Siegel MP, Kruse SE, Percival JM, Goh J, White CC, Hopkins HC, Kavanagh TJ, Szeto HH, Rabinovitch PS, and Marcinek DJ. Mitochondrial-targeted peptide rapidly improves mitochondrial energetics and skeletal muscle performance in aged mice. *Aging Cell* 12: 763–771, 2013.
67. Siegel MP, Wilbur T, Mathis M, Shankland EG, Trieu A, Harper ME, and Marcinek DJ. Impaired adaptability of in vivo mitochondrial energetics to acute oxidative insult in aged skeletal muscle. *Mech Ageing Dev* 133: 620–628, 2012.
68. Silvagno F, Xia H, and Bredt DS. Neuronal nitric-oxide synthase-mu, an alternatively spliced isoform expressed in differentiated skeletal muscle. *J Biol Chem* 271: 11204–11208, 1996.
69. Sips PY and Buys ES. Genetic modification of hypertension by sGCalpha1. *Trends Cardiovasc Med* 23: 312–318, 2013.
70. Stasch JP, Becker EM, Alonso-Alija C, Apeler H, Dembowsky K, Feurer A, Gerzer R, Minuth T, Perzborn E, Pleiss U, Schroder H, Schroeder W, Stahl E, Steinke W, Straub A, and Schramm M. NO-independent regulatory site on soluble guanylate cyclase. *Nature* 410: 212–215, 2001.
71. Suzuki N, Motohashi N, Uezumi A, Fukada S, Yoshimura T, Itoyama Y, Aoki M, Miyagoe-Suzuki Y, and Takeda S. NO production results in suspension-induced muscle atrophy through dislocation of neuronal NOS. *J Clin Invest* 117: 2468–2476, 2007.
72. Thomas GD, Shaul PW, Yuhanna IS, Froehner SC, and Adams ME. Vasomodulation by skeletal muscle-derived nitric oxide requires alpha-syntrophin-mediated sarcolemmal localization of neuronal Nitric oxide synthase. *Circ Res* 92: 554–560, 2003.

Address correspondence to:
Dr. Justin M. Percival
Department of Molecular and Cellular Pharmacology (R-189)
University of Miami Miller School of Medicine
PO Box 016189
Miami, FL 33101

E-mail: j.percival@med.miami.edu

Date of first submission to ARS Central, January 6, 2016; date of final revised submission, June 16, 2016; date of acceptance, June 28, 2016.

Abbreviations Used

α1GC = α1 soluble guanylate cyclase subunit
α2GC = α2 soluble guanylate cyclase subunit
β1GC = β1 soluble guanylate cyclase subunit
AchR = acetylcholine receptor
ATP = adenosine triphosphate
ATP5a = mitochondrial ATP synthase alpha-subunit
cGMP = cyclic guanosine monophosphate
DETANO = diethylenetriamine NONOate
DEXA = dual-energy X-ray absorptiometry
Dia = diaphragm
DBMD = Duchenne/Becker muscular dystrophy
DMD = Duchenne muscular dystrophy
Gas = gastrocnemius
GC = soluble guanylate cyclase
GC1 = soluble guanylate cyclase 1 comprising α1 and β1 guanylate cyclase subunits
GC2 = soluble guanylate cyclase 2 comprising α2 and β1 guanylate cyclase subunits
GM130 = 130kDa cis-Golgi matrix protein
GTP = guanosine 5′-triphosphate
IFM = intermyofibrillar mitochondria
L-NAME = L-N^G-nitroarginine methyl ester
MTCO1 = mitochondrial cytochrome C oxidase 1
MuRF1 = muscle-specific RING finger protein 1
NDUFB8 = NADH dehydrogenase 1 beta subcomplex, 8
NO = nitric oxide
nNOS = neuronal nitric oxide synthase
PDE5 = phosphodiesterase 5
PGC1α = peroxisome proliferator-activated receptor, gamma, coactivator 1, alpha
PKG = cGMP-activated protein kinase
Quad = quadriceps
SDHB = succinate dehydrogenase complex, subunit B
Sol = soleus
SSM = subsarcolemmal mitochondria
TA = tibialis anterior
UQCRC2 = ubiquinol–cytochrome c reductase core protein II
VDAC1 = voltage-dependent anion channel 1